THE INSTABILITY OF FLUIDS WITH TIME DEPENDENT HEATING

Thesis by

Iain George Currie

In Partial Fulfillment of the Requirements

For the Degree of

Doctor of Philosophy

California Institute of Technology

Pasadena, California

1966

(Submitted May 20, 1966)

ACKNOWLEDGMENTS

My sincere thanks are extended to Dr. W. D. Rannie for his valuable guidance and advice during the course of this research.

Financial support for this project was provided, in part, by the National Science Foundation, and this aid is most gratefully acknowledged.

Finally, the author would like to acknowledge the cooperation of the staff of the California Institute of Technology, in particular Mrs. Roberta Duffy, who typed this thesis.

ABSTRACT

The stability of a fluid having a non-uniform temperature stratification is examined analytically for the response of infinitesimal disturbances. The growth rates of disturbances have been established for a semi-infinite fluid for Rayleigh numbers of 10^3, 10^4, and 10^5 and for Prandtl numbers of 7.0 and 0.7.

The critical Rayleigh number for a semi-infinite fluid, based on the effective fluid depth, is found to be 32, while it is shown that for a finite fluid layer the critical Rayleigh number depends on the rate of heating. The minimum critical Rayleigh number, based on the depth of the fluid layer, is found to be 1340.

The stability of a finite fluid layer is examined for two special forms of heating. The first is constant flux heating, while in the second, the temperature of the lower surface is increased uniformly in time. In both cases, it is shown that for moderate rates of heating the critical Rayleigh number is reduced, over the value for very slow heating, while for very rapid heating the critical Rayleigh number is greatly increased. These results agree with published experimental observations.

The question of steady, non-cellular convection is given qualitative consideration. It is concluded that, although the motion may originate from infinitesimal disturbances during non-uniform heating, the final flow field is intrinsically non-linear.

TABLE OF CONTENTS

Part	Title	Page
	Acknowledgments	ii
	Abstract	iii
	Table of Contents	iv
	List of Figures	v
	List of Tables	vi
	List of Symbols	vii
I.	INTRODUCTION	1
II.	THEORY AND ANALYSIS	8
	1. Governing Equations	8
	2. Perturbation Equations	10
	3. Time Dependence	13
	4. Conduction Temperature Profile	15
	5. Boundary Conditions	18
	6. Solution of Eigenvalue Problem	20
	7. Marginal Stability	27
III.	RESULTS AND DISCUSSION	31
	1. Behavior of Determinant	31
	2. Growth Rates of Disturbances	37
	3. Velocity and Temperature Profiles	47
	4. Critical Rayleigh Number	53
IV.	COMPARISON WITH EXPERIMENTS	62
	1. Review of Experimental Results	62
	2. Constant Flux Heating	67
	3. Uniformly Increasing Temperature	71
	4. Maintained Non-Cellular Convection	76
V.	SUMMARY AND CONCLUSIONS	79
	References	82

LIST OF FIGURES

Figure No.	Title	Page
1	Conduction Temperature Profile	16
2	Approximation to Temperature Profile	16
3	Behavior of Determinant	34
4	Growth Rate of Disturbances	38
5	Growth Rate of Disturbances	39
6	Growth Rate of Disturbances	40
7	Growth Rate of Disturbances	41
8	Growth Rate of Disturbances	42
9	Growth Rate of Disturbances	43
10	Growth Rate of Disturbances	44
11	Velocity Profile	48
12	Temperature Profile	49
13	Velocity Profile	51
14	Temperature Profile	52
15	Determination of Critical Rayleigh Number	54
16	Critical Rayleigh Number	56
17	Critical Wave Number	57
18	Nature of Boundaries for Finite Fluid Layer	59
19	Critical Rayleigh Number	60
20	Critical Wave Number	61
21	Data for Maintained Columnar Convection	63
22	Stability Curve for Constant Flux Heating	69
23a	Stability Curve for Uniformly Increasing Temperature	73
23b	Stability Curve for Uniformly Increasing Temperature	74

LIST OF TABLES

Table No.	Title	Page
I	Wave Numbers of Fastest Growing Disturbances	45
II	Data for Onset of Instability in Evaporating Water	75

LIST OF SYMBOLS

a	Wave number based on effective depth, d
$\tilde{a}$	Wave number based on fluid depth, h
A	Parameter, defined following equation (44)
B	Parameter, defined following equation (44)
C_i	Constants of integration
C_p	Specific heat at constant pressure
d	Effective depth, defined in Figure 2
D	Differential operator = d/dz
F	Froude number = $\bar{U}^2/gd$
g	Acceleration due to gravity
h	Depth of finite fluid layer
k	Thermal conductivity
$\underline{k}$	Unit vector in upward vertical direction
p	Pressure
P	Prandtl number = $(C_p\mu)/k$
Pe	Peclet number = $(\rho\bar{U}dC_p)/k$
Q	Heat flux
R	Rayleigh number = $[\alpha g(T_o^*-T_1^*)d^3]/\varkappa\nu$
$\tilde{R}$	Rayleigh number = $[\alpha g(T_o^*-T_1^*)h^3]/\varkappa\nu$
t	Time
T	Temperature
T_o	Temperature at lower surface
T_1	Temperature at infinity or at upper surface
$\bar{U}$	Characteristic velocity

u, v, w	Velocity components
U, V, W	Velocity components
x, y, z	Independent Cartesian coordinates
α	Coefficient of thermal expansion
β	Parameter = $(2a^2 + \frac{\sigma}{P})$
β_1	Heating parameter
γ_i	Exponential indices
$\overline{\gamma}$	$i\gamma$
δ	Wave length
ϵ	Effective depth ratio = d/h
ζ	Thickness ratio = h/d
θ	Temperature
$\varkappa$	Thermal diffusivity = $k/(\rho C_p)$
λ_i	Exponential indices
μ	Absolute viscosity
ν	Kinematic viscosity
ρ	Density
ρ_1	Density at temperature T_1
σ	Growth rate of disturbances
σ_o	Value of σ defined by equation (52)
σ_1	Value of σ defined by equation (50)
σ_a	Growth rate of disturbances in air
σ_w	Growth rate of disturbances in water
τ	Parameter = $a^2(a^2 + \frac{\sigma}{P})$
ω	Velocity

Superscripts:

*	Dimensional
(o)	Conduction phase
(1)	Perturbation phase

Subscripts:

c	Corresponding to marginal stability of fastest growing wave

I. INTRODUCTION

When a stationary fluid develops a density stratification, an instability may occur which results in motion of the fluid. The sustained form of this motion consists of vertical convective currents which are repeated horizontally at intervals. A number of experimental investigations of this motion have been carried out, usually involving a thin layer of fluid in the laboratory.

The first writing on the above subject is due to Thomson (1882) who made observations of thermal convection currents in water. It was noted that the convection developed a cellular structure and Thomson associated the entire process with the evaporative cooling of the upper surface.

Detailed measurements were first made by Benard (1900, 1901) who used a finite fluid layer whose depth could be varied. The structure of the cells was examined visually and values of the temperature difference across the bounding surfaces at the onset of convection were measured and recorded. The cell planforms were found to be predominantly hexagonal, but a few two-dimensional rolls were also observed.

The rate of heat transfer, both before and after the initiation of convective motion, was measured by Schmidt and Milverton (1935). A break in the slope of the curve of heat transfer rate versus temperature difference was obtained, the heat transfer rate being higher in the convection mode than in the conduction mode. Malkus (1954) observed discrete transitions in the heat transfer rate at six

different values of the impressed temperature difference. These transitions were attributed to changes from conduction to laminar convection to different modes of turbulent convection. Using schlieren photography, Silveston (1958) confirmed these basic modes of heat transfer.

Schmidt and Saunders (1938) measured the ratio of the length of the horizontal side to the depth of the convection cells. They found this ratio to be about two.

The different geometrical forms assumed by the convection cells were examined by Benard and Avsec (1938). These authors also discuss the applications of thermal instability to the fields of astronomy and meteorology. A series of papers on such applications appears in the publication edited by Miner (1947).

The direction of vertical motion of cellular convection in liquid sulphur was shown by von Tippelskirch (1956) to reverse at about 153°C. Since the variation of viscosity with temperature also reverses at this point, it was concluded that the flow in the center of the cells takes place in the direction of increasing viscosity, a situation first postulated by Graham (1933).

Foster (1965b) carried out experiments in a layer of water which was cooled from above by surface evaporation. It was found that the time required for disturbances to grow, and the wave number of the fastest growing disturbances, were independent of the depth of the fluid.

Complementary to the foregoing experimental studies, significant analytical advances have been made in understanding the

various physical phenomena which have been observed. The first analytical work was carried out by Rayleigh (1916), who showed that the onset of convection depended on the value of a dimensionless group which is now known as the Rayleigh number. A critical value of 657.5 was obtained for this parameter for a fluid layer having two free boundaries. The principle of the exchange of stabilities was also established by Rayleigh for this case. That is, it was shown that disturbances must grow aperiodically in time and that marginal stability corresponds to a stationary flow pattern.

The value of 657.5 for the critical Rayleigh number is substantially lower than the experimentally observed value of about 1700. Jeffreys (1926, 1928) showed that if the boundaries are considered as rigid, the numerical value of the critical Rayleigh number becomes 1707.8. This numerical value was refined by Low (1929), and the effect of various types of boundary conditions was studied by Sparrow, Goldstein, and Jonsson (1964).

It was shown by Jeffreys (1930) that the incompressible analysis may be used for compressible fluids, provided the temperature gradient is interpreted as the difference between the adiabatic temperature gradient and the prevailing temperature gradient.

The principle of the exchange of stabilities was established by Pellew and Southwell (1940) for the case of two rigid boundaries and for the case of one rigid and one free boundary. A critical Rayleigh number of 1100.7 was obtained for the latter case.

The stability of a fluid layer which is bounded by stable regions of the same fluid was examined by Gribov and Gurevich (1957). For

small Rayleigh numbers it was found that the mixing region was small for upward convection only, but that for both upward and downward penetration the mixing region could be large. Such penetration was also investigated by Veronis (1963).

The importance of viscosity and thermal conductivity in fluid instability was examined by Morton (1957). The initial growth rate of disturbances was also calculated and was shown to depend on both the Rayleigh number and the Prandtl number.

The amplitude of the velocity and temperature perturbations, as given by the linearized stability theory, was established by Malkus and Veronis (1958). This enabled the rate of heat transfer to be calculated and the distortions of the linearized flow fields due to finite amplitude effects was examined. The amplitude of the perturbations was also calculated by Gorkov (1958) and by Nakagawa (1960),and the rate of heat transfer was studied by Kuo (1961).

The variation of viscosity with temperature was considered by Palm (1960) who found that the critical Rayleigh number was slightly less than for the constant viscosity case. The various waves were also found to interact in such a way that hexagonal cells result. The stability of the maintained mode of convection has been subsequently examined by Segel and Stuart (1962), Segel (1962, 1965a, 1965b) and by Palm and Øiann (1964).

Apart from the foregoing results, which refer to the simplest examples of the basic phenomena, some work has been done on the effects of shear motion, rotation, and acceleration of the fluid medium as well as the effects of surface tension and impressed magnetic

fields. References to most of these works are to be found in the book by Chandrasekhar (1961).

The results reported above appear to form a comprehensive and consistent understanding of the phenomena associated with thermally induced fluid instability. However, certain anomalies have been observed from time to time which have not been explained analytically.

It was observed by Graham (1933) that a columnar mode of instability may be established at smaller Rayleigh numbers than required for cellular instability, but no numerical data was recorded. Measurements of the minimum temperature differences for maintained convection were recorded by Chandra (1938) and by Dassanayake, the latter results being published by Sutton (1950). These temperature differences were considerably smaller than the theoretical values for criticality. It was suggested by Sutton that the cause of this new mode of instability may be the non-linear form of the conduction temperature profile during the initial stages of heating. This would be a direct violation of one of the basic assumptions of the analyses.

The rate of heat transfer across a fluid layer with two rigid boundaries was measured by de Graaf and van der Held (1953). They observed that thermal convection could be initiated at Rayleigh numbers in excess of about 1400, rather than 1707.8, and agreed with Sutton that the rate of heating might be important in accounting for the discrepancy.

Soberman (1959) measured the critical Rayleigh number for a range of heating rates. He found that the heating rate did indeed

influence the critical Rayleigh number and recorded values of $\tilde{R}_c$ as high as 3×10^4. It was found that the curve $\tilde{R}_c = 90.7(\frac{\alpha g Q h^4}{2\kappa\nu k})^{0.394}$ correlated his data, which was for one fixed and one free surface.

Using schlieren photography, Spangenberg and Rowland (1961) recorded the temperature profile in a layer of water which was cooled by evaporation at the upper surface. The results showed that the temperature profile at criticality was a highly non-linear function of the spatial coordinate and that a stationary mode of motion could be maintained at a considerably lower Rayleigh number than that corresponding to the onset of instability.

No analytical explanation of the foregoing phenomena has been given, and only a few studies have been made of the apparent related effects. Morton (1957), using approximate methods, concluded that a slightly non-linear temperature profile would have a negligible effect on the critical Rayleigh number. Again, Sparrow, Goldstein, and Jonsson (1964) found that, for a particular type of distributed body heat source, disturbances behaved very differently when a non-linear temperature distribution existed.

Some numerical work has been performed which sheds some light on the nature of the sustained flow fields. Herring (1963) accounted for the principal non-linear terms and solved the stability equation as an initial value problem using numerical methods. The steady temperature profile showed a strong boundary layering effect near the bounding surfaces. Fromm (1965) solved the two-dimensional non-linear equations by a finite difference method and obtained similar results.

The manifestation time of disturbances was investigated numerically by Foster (1965a) for an initially homogeneous fluid layer with two free boundaries. The results showed that, for large Rayleigh numbers, the manifestation time and the wave numbers of the fastest growing disturbances are independent of the fluid depth.

Lick (1965) analyzed the effect of a strong variation of temperature with depth in a finite fluid layer and found that, for large Rayleigh numbers, disturbances could grow much faster than they would in a uniform temperature stratification.

The present investigation is directed towards obtaining an understanding of some of the latter anomalies. In particular, the role of a strong non-linear temperature stratification has not been fully investigated. Since, in a finite fluid, the strongest temperature non-linearities occur in the early stages of heating, when the effect of the upper boundary is not felt, it seems desirable to investigate this effect for a semi-infinite fluid field. In this way, we will obtain those results for a semi-infinite fluid which cannot be obtained from the results for a finite fluid in the limit of the depth becoming infinite.

We may ask how rapidly disturbances grow and what mode the resulting motion assumes. We would also like to know what the conditions are for marginal stability. Specifically, we would inquire whether the rate of heating influences marginal stability, and if so, to what extent and in what manner. Finally, we might ask why a sustained mode of convection has been observed at a significantly lower Rayleigh number than that predicted by the existing theory.

II. THEORY AND ANALYSIS

1. Governing Equations

When a fluid is heated from below, the lowest layers become less dense due to the thermal expansion of the fluid. Thus, the buoyancy force tends to drive the less dense fluid upwards and to replace it with the colder, more dense fluid from above. However, the motion associated with such an exchange is inhibited by the viscosity of the fluid, so that some critical temperature gradient must be attained before such a motion will begin. Thus, the analysis should account for the variation of density with temperature as well as the effects of viscosity and heat conductivity. However, since only relatively small temperature differences are encountered, the Boussinesq approximation will be used. This approximation states that the changes of density are relatively unimportant, except in the body force term of the momentum equation. Thus, the governing equations are

$$\nabla \cdot \underline{u}^* = 0 \tag{1}$$

$$\frac{\partial \underline{u}^*}{\partial t^*} + \underline{u}^* \cdot \nabla \underline{u}^* = -\frac{1}{\rho_1} \nabla p^* + \nu \nabla^2 \underline{u}^* - g\{1-\alpha(T^*-T_1^*)\}\underline{k} \tag{2}$$

$$\frac{\partial T^*}{\partial t^*} + \underline{u}^* \cdot \nabla T^* = \kappa \nabla^2 T^* \tag{3}$$

where we have written for the density

$$\rho = \rho_1\{1-\alpha(T^*-T_1^*)\} \ .$$

It is convenient to introduce dimensionless variables at this point. We introduce new independent variables defined by

$$x = x^*/d \qquad y = y^*/d \qquad z = z^*/d \qquad t = \frac{\kappa}{d^2} t^*$$

and new dependent variables defined by

$$u = \frac{d}{\varkappa} u^* \qquad v = \frac{d}{\varkappa} v^* \qquad w = \frac{d}{\varkappa} w^* \qquad p = \frac{d^2}{\varkappa^2} \frac{p^*}{\rho_1} \qquad T = \frac{g\alpha d^3}{\varkappa\nu} T^* \ .$$

The characteristic length d will be discussed later. In terms of these new variables, equations (1), (2), and (3) become

$$\nabla \cdot \underline{u} = 0 \tag{4}$$

$$\frac{\partial \underline{u}}{\partial t} + \underline{u} \cdot \nabla \underline{u} = - \nabla p + P\nabla^2 \underline{u} - \left\{ \frac{P_e^2}{F} - P(T-T_1) \right\} \underline{k} \tag{5}$$

$$\frac{\partial T}{\partial t} + \underline{u} \cdot \nabla T = \nabla^2 T \ . \tag{6}$$

2. Perturbation Equations

In the initial state the transfer of heat is by conduction alone so that the fluid remains at rest. Furthermore, since the heating is uniform with respect to some plane, say $z = 0$, the temperature and pressure will be functions of z and t only, independent of x and y. Then the equations governing the unperturbed state are

$$\underline{u}^{(o)} = 0 \tag{7}$$

$$\frac{\partial p^{(o)}}{\partial z} = -\frac{P_e^2}{F} + P\left(T^{(o)} - T_1\right) \tag{8}$$

$$\frac{\partial T^{(o)}}{\partial t} = \frac{\partial^2 T^{(o)}}{\partial z^2} \tag{9}$$

We now allow this initial state to suffer a small perturbation so that

$$\underline{u} = \underline{u}^{(1)} \tag{10}$$

$$T = T^{(o)} + T^{(1)} \tag{11}$$

$$p = p^{(o)} + p^{(1)} \tag{12}$$

where $T^{(1)} \ll T^{(o)}$, $p^{(1)} \ll p^{(o)}$, and $\underline{u}^{(1)} \sim T^{(1)}, p^{(1)}$. Substituting equations (10), (11), and (12) into equations (4), (5), and (6) and making use of equations (7), (8), and (9), we arrive at the perturbation equations.

$$\nabla \cdot \underline{u}^{(1)} = 0 \tag{13}$$

$$\frac{\partial \underline{u}^{(1)}}{\partial t} = -\nabla p^{(1)} + P\nabla^2 \underline{u}^{(1)} + PT^{(1)}\underline{k} \tag{14}$$

$$\frac{\partial T^{(1)}}{\partial t} + w^{(1)} \frac{\partial T^{(o)}}{\partial z} = \nabla^2 T^{(1)} \tag{15}$$

The pressure can be eliminated from the analysis by making use of the identities

$$\nabla \times \nabla p = 0 \ , \qquad \nabla \times (\nabla \times \underline{u}) = \nabla(\nabla \cdot \underline{u}) - \nabla^2 \underline{u} \ .$$

Thus, taking the curl of equation (14) and making use of equation (13), we have

$$\frac{\partial}{\partial t}\nabla^2 \underline{u}^{(1)} = P\nabla^4 \underline{u}^{(1)} + P\left(\nabla^2 T^{(1)}\underline{k} - \nabla \frac{\partial T^{(1)}}{\partial z}\right) .$$

The transverse velocity components can also be eliminated now by taking the scalar product of this equation with the unit vector $\underline{k}$. The resulting equation, together with equation (15), gives the following two equations in $w^{(1)}$ and $T^{(1)}$.

$$\left(\nabla^2 - \frac{1}{P}\frac{\partial}{\partial t}\right)\nabla^2 w^{(1)} = -\nabla_{xy}^2 T^{(1)} \tag{16}$$

$$\left(\nabla^2 - \frac{\partial}{\partial t}\right)T^{(1)} = \frac{\partial T^{(o)}}{\partial z} w^{(1)} \tag{17}$$

Since we are considering an arbitrary disturbance, we can represent $w^{(1)}$ and $T^{(1)}$ by Fourier integrals. That is, we look for solutions of the form

$$w^{(1)}(x, y, z, t) = \int_{-\infty}^{\infty}\int_{-\infty}^{\infty} \omega(z, t) e^{i(a_x x + a_y y)} da_x da_y$$

$$T^{(1)}(x, y, z, t) = \int_{-\infty}^{\infty}\int_{-\infty}^{\infty} \theta(z, t) e^{i(a_x x + a_y y)} da_x da_y$$

and since we are studying the stability of the system for all wave numbers, equations (16) and (17) give

$$\left(\frac{\partial^2}{\partial z^2} - a^2 - \frac{1}{P}\frac{\partial}{\partial t}\right)\left(\frac{\partial^2}{\partial z^2} - a^2\right)\omega = a^2\theta \tag{18}$$

$$\left(\frac{\partial^2}{\partial z^2} - a^2 - \frac{\partial}{\partial t}\right)\theta = \frac{\partial T^{(o)}}{\partial z}\omega \tag{19}$$

where $a = \sqrt{a_x^2 + a_y^2}$.

The analysis is most conveniently performed in terms of the

longitudinal velocity w, so we eliminate θ from equations (18) and (19) to obtain an equation in w only.

$$\left(\frac{\partial^2}{\partial z^2} - a^2\right)\left(\frac{\partial^2}{dz^2} - a^2 - \frac{\partial}{\partial t}\right)\left(\frac{\partial^2}{\partial z^2} - a^2 - \frac{1}{P}\frac{\partial}{\partial t}\right)w = a^2 \frac{\partial T^{(o)}}{\partial z} w \quad (20)$$

Once we have solved for w, θ can be obtained from equation (18).

Equation (20) is a partial differential equation for w in z and t. Furthermore, since $\partial T^{(o)}/\partial z$ will depend on z and t, the coefficients are not constant and the variables do not separate. It is therefore desirable to introduce approximations which will facilitate the analysis.

3. Time Dependence

If we restrict ourselves to the initial growth stages of an arbitrary disturbance, it will be sufficient to consider only a very short time interval and to inquire whether the disturbance is growing, decaying, or is stationary during this brief period. From solutions of the heat conduction equation we know that the time required for the temperature profile to change by a factor of $1/e$ is d^2/κ. Thus, if we consider time intervals which are small compared with d^2/κ, we may neglect the variation of $\partial T^{(o)}/\partial z$ with time. That is, for $t^* \ll d^2/\kappa$, or $t \ll 1$, we may replace $\partial T^{(o)}/\partial z$ by $dT^{(o)}/dz$, the latter being a function of z only. Under these circumstances, the coefficients of equation (20) are independent of t so that the time dependence is given by $e^{\sigma t}$. Specifically, we write

$$w(z,t) = W(z)e^{\sigma t} \tag{21}$$

$$\theta(z,t) = T(z)e^{\sigma t} \tag{22}$$

Then from equations (20) and (18) we have, respectively,

$$(D^2-a^2)(D^2-a^2-\sigma)\left(D^2-a^2-\frac{\sigma}{P}\right)W = a^2 \frac{dT^{(o)}}{dz} W \tag{23}$$

$$a^2 T = (D^2-a^2)\left(D^2-a^2-\frac{\sigma}{P}\right)W \tag{24}$$

where we have introduced the operator $D = d/dz$.

The reason for choosing the time scale d^2/κ now becomes apparent. In the present analysis, the time scale d^2/κ is much more meaningful than the time scale d^2/ν, which is usually used in similar stability calculations.

We have succeeded in reducing the stability equation to the ordinary differential equation (23), but this equation has non-constant

coefficients due to the factor $dT^{(o)}/dz$ which is still a function of z in general. Although a series solution could be sought, such a solution would require elaborate numerical exploration of the special functions so defined. Moreover, these functions would be different for each form of $dT^{(o)}/dz$. It is therefore proposed to introduce an additional simplification.

4. Conduction Temperature Profile

In the conduction phase, the temperature $T^{(o)}$ must satisfy equation (9). As such, the profile will be as shown in Figure 1 for $t \ll 1$ after onset of heating at $t = 0$.

A most useful approximation, which was used by Lick, is to represent the temperature profile by two straight line segments. For a semi-infinite fluid we accomplish this in the manner shown in Figure 2. The depth d is chosen such that the area under the actual and approximate curves is the same. This assures that the total buoyancy force is preserved. The temperature gradient in the upper region is zero, while in the lower region it is given by $(T_o^* - T_1^*)/d$ so that $dT^{(o)}/dz = -(T_o - T_1) = -R$. Then from equations (23) and (24) we have

$$(D^2-a^2)(D^2-a^2-\sigma)(D^2-a^2-\frac{\sigma}{P})W_1 = -a^2 R W_1 \tag{25}$$

$$(D^2-a^2)(D^2-a^2-\sigma)(D^2-a^2-\frac{\sigma}{P})W_2 = 0 \tag{26}$$

$$a^2 T_1 = (D^2-a^2)(D^2-a^2-\frac{\sigma}{P})W_1 \tag{27}$$

$$a^2 T_2 = (D^2-a^2)(D^2-a^2-\frac{\sigma}{P})W_2 \tag{28}$$

The length scale d, which was introduced earlier, has now been defined and equation (23) has been replaced by equations (25) and (26), both of which have constant coefficients. Then the solutions to these equations will be of the form $W_1 \sim e^{\gamma z}$ and $W_2 \sim e^{\lambda z}$. Thus, from equations (25) and (26) we have, for distinct γ's and λ's,

$$W_1 = C_1 e^{-\gamma_1 z} + C_2 e^{-\gamma_2 z} + C_3 e^{-\gamma_3 z} + C_4 e^{\gamma_1 z} + C_5 e^{\gamma_2 z} + C_6 e^{\gamma_3 z} \tag{29}$$

$$W_2 = C_7 e^{-\lambda_1 z} + C_8 e^{-\lambda_2 z} + C_9 e^{-\lambda_3 z} + C_{10} e^{\lambda_1 z} + C_{11} e^{\lambda_2 z} + C_{12} e^{\lambda_3 z} \tag{30}$$

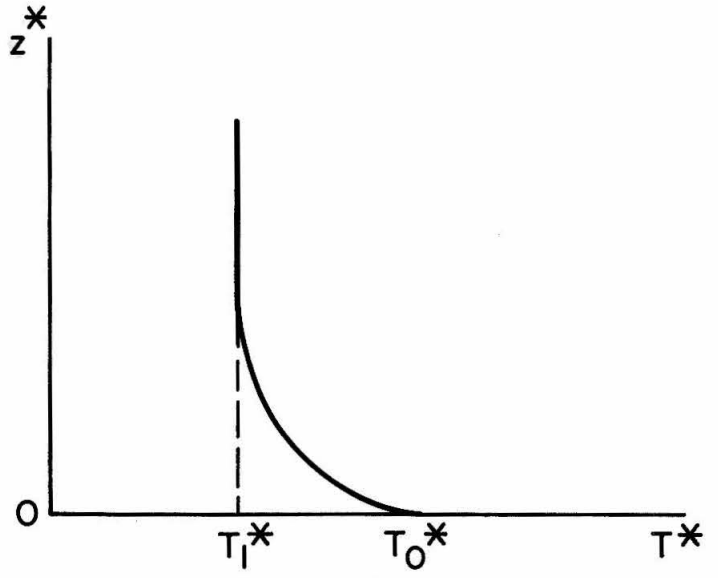

FIGURE 1 – CONDUCTION TEMPERATURE PROFILE

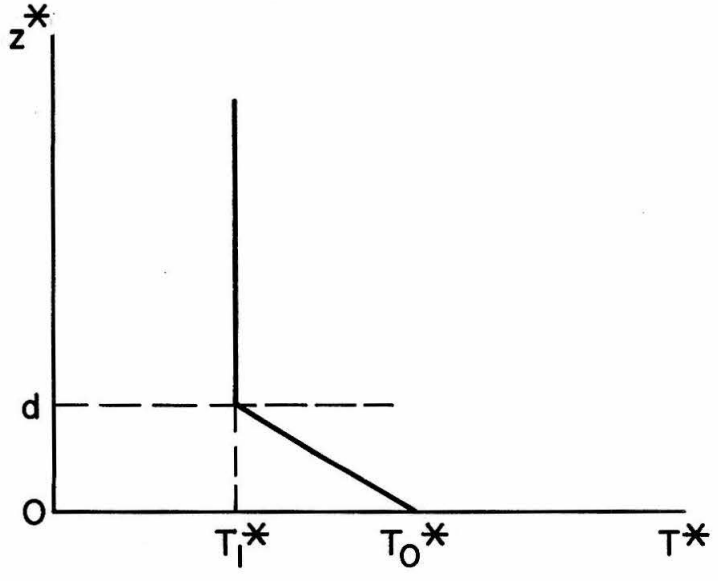

FIGURE 2 – APPROXIMATION TO TEMPERATURE PROFILE

where the γ's and λ's satisfy the equations

$$(\gamma^2-a^2)(\gamma^2-a^2-\sigma)(\gamma^2-a^2-\frac{\sigma}{P}) = -a^2R \qquad (31)$$

$$(\lambda^2-a^2)(\lambda^2-a^2-\sigma)(\lambda^2-a^2-\frac{\sigma}{P}) = 0 \qquad (32)$$

The mathematical model introduced in this section has a physical interpretation. Replacing the actual temperature profile by two straight-line segments of unequal gradients is equivalent to locating a heat sink along the plane $z = 1$. Since the temperature gradient in the upper region is zero, the strength of the heat sink is such that it absorbs all the heat approaching it from below in the conduction phase. That is, when a particular conduction profile has been chosen and the associated depth d calculated, the strength of the heat sink is uniquely determined. Any perturbation to the temperature profile will result in a heat flux through the plane $z = 1$ due to the fixed nature of the heat sink.

The time dependence of the previous section is exact for all values of t for this mathematical model. It is only when the results of the analysis are applied to the physical problem that the restriction $t \ll 1$ must be observed.

5. Boundary Conditions

We must now define the basic boundary conditions and, since the analysis has been carried out in terms of the longitudinal velocity W, we must interpret them in terms of W.

Performing the same Fourier and time analyses on the transverse velocity components and the pressure as we performed on the longitudinal velocity and the temperature, equations (13) and (14) give

$$ia_x U + ia_y V + DW = 0 \tag{33}$$

$$\sigma U = -ia_x p + P(D^2 - a^2)U \tag{34}$$

$$\sigma V = -ia_y p + P(D^2 - a^2)V \tag{35}$$

On the plane $z = 0$ we have a rigid boundary so that $W_1 = 0$. Also, $U = V = 0$, so that from equation (33) we have the condition that $DW_1 = 0$. Further, since the temperature is prescribed on $z = 0$, the temperature perturbation T_1 must vanish there. Then from equation (27) we have that $D^2(D^2 - 2a^2 - \frac{\sigma}{P})W_1 = 0$. Thus, we have established the following boundary conditions.

On $z = 0$;

$$W_1 = DW_1 = D^2(D^2 - 2a^2 - \frac{\sigma}{P})W_1 = 0 \tag{36}$$

At the interface of the two regions we require continuity of the velocity, stress, and heat flux components as well as continuity of the temperature. Continuity of the velocity gives immediately that $W_1 = W_2$ on $z = 1$. Also, equation (33) shows that $DW_1 = DW_2$. Continuity of the tangential stresses requires that DU and DV be continuous so that applying the operator D to equation (33) shows that $D^2W_1 = D^2W_2$. Equations (34) and (35) show that D^2U and D^2V are continuous so that

applying the operator D^2 to equation (33) establishes the condition that $D^3W_1 = D^3W_2$. Since the temperature is continuous, equation (24) now requires that $D^4W_1 = D^4W_2$, and since the perturbation heat flux is also continuous, the same equation requires that $D^5W_1 = D^5W_2$. Then our boundary conditions at the interface are:

on $z = 1$;

$$(W_1 - W_2) = (D^nW_1 - D^nW_2) = 0 \qquad n = 1, 2, 3, 4, 5 \tag{37}$$

For very large values of z we require that the velocity and temperature perturbations, as well as their derivatives, should vanish. That is,

as $z \to \infty$;

$$W_2 \to 0 \qquad \text{and} \qquad D^nW_2 \to 0 \ . \tag{38}$$

The general solutions (29) and (30), together with the boundary conditions (36), (37), and (38), define an eigenvalue problem.

6. Solution of Eigenvalue Problem

Equation (31) is a sixth order equation in γ, but since only even powers of γ appear, it can be considered a cubic equation in γ^2. Using the formulas for the solution of a cubic equation together with equations (31) and (32) we arrive at expressions for the γ's and λ's.

$$\gamma_1 = \left[a^2 + \frac{1}{3}\left(1 + \frac{1}{P}\right)\sigma + A + B\right]^{\frac{1}{2}} \tag{39}$$

$$\gamma_2 = \left[a^2 + \frac{1}{3}\left(1 + \frac{1}{P}\right)\sigma - \frac{1}{2}(A+B) + i\,\frac{\sqrt{3}}{2}(A-B)\right]^{\frac{1}{2}} \tag{40}$$

$$\gamma_3 = \left[a^2 + \frac{1}{3}\left(1 + \frac{1}{P}\right)\sigma - \frac{1}{2}(A+B) - i\,\frac{\sqrt{3}}{2}(A-B)\right]^{\frac{1}{2}} \tag{41}$$

$$\lambda_1 = a \tag{42}$$

$$\lambda_2 = (a^2 + \sigma)^{\frac{1}{2}} \tag{43}$$

$$\lambda_3 = \left(a^2 + \frac{\sigma}{P}\right)^{\frac{1}{2}} \tag{44}$$

where A and B are defined by

$$A = \left\{\frac{1}{54}\left(1+\frac{1}{P}\right)\left(2-\frac{1}{P}\right)\left(1-\frac{2}{P}\right)\sigma^3 - \frac{1}{2}a^2R + \left[\frac{1}{4}a^4R^2 - \frac{a^2R}{54}\left(1+\frac{1}{P}\right)\left(2-\frac{1}{P}\right)\times \left(1-\frac{2}{P}\right)\sigma^3 - \frac{1}{108P^2}\left(1-\frac{1}{P}\right)^2\sigma^6\right]^{1/2}\right\}^{1/3}$$

$$B = \left\{\frac{1}{54}\left(1+\frac{1}{P}\right)\left(2-\frac{1}{P}\right)\left(1-\frac{2}{P}\right)\sigma^3 - \frac{1}{2}a^2R - \left[\frac{1}{4}a^4R^2 - \frac{a^2R}{54}\left(1+\frac{1}{P}\right)\left(2-\frac{1}{P}\right)\left(1-\frac{2}{P}\right)\sigma^3 - \frac{1}{108P^2}\left(1-\frac{1}{P}\right)^2\sigma^6\right]^{1/2}\right\}^{1/3}$$

The boundary conditions (38) and the solution (30) immediately require that $C_{10} = C_{11} = C_{12} = 0$ in view of the fact that the λ's are all positive as defined by equations (42), (43), and (44). The remaining boundary conditions (36) and (37), together with the solutions (29)

and (30), result in the following system of algebraic equations to be solved for the arbitrary constants.

$$C_1 + C_2 + C_3 + C_4 + C_5 + C_6 = 0$$

$$-\gamma_1 C_1 - \gamma_2 C_2 - \gamma_3 C_3 + \gamma_1 C_4 + \gamma_2 C_5 + \gamma_3 C_6 = 0$$

$$\gamma_1^2(\gamma_1^2-\beta)C_1+\gamma_2^2(\gamma_2^2-\beta)C_2+\gamma_3^2(\gamma_3^2-\beta)C_3+\gamma_1^2(\gamma_1^2-\beta)C_4+\gamma_2^2(\gamma_2^2-\beta)C_5+$$
$$\gamma_3^2(\gamma_3^2-\beta)C_6 = 0$$

$$e^{-\gamma_1}C_1+e^{-\gamma_2}C_2+e^{-\gamma_3}C_3+e^{\gamma_1}C_4+e^{\gamma_2}C_5+e^{\gamma_3}C_6-e^{-\lambda_1}C_7-e^{-\lambda_2}C_8$$
$$-e^{-\lambda_3}C_9 = 0$$

$$-\gamma_1 e^{-\gamma_1}C_1-\gamma_2 e^{-\gamma_2}C_2-\gamma_3 e^{-\gamma_3}C_3+\gamma_1 e^{\gamma_1}C_4+\gamma_2 e^{\gamma_2}C_5+\gamma_3 e^{\gamma_3}C_6$$
$$+\lambda_1 e^{-\lambda_1}C_7+\lambda_2 e^{-\lambda_2}C_8+\lambda_3 e^{-\lambda_3}C_9 = 0$$

$$\gamma_1^2 e^{-\gamma_1}C_1+\gamma_2^2 e^{-\gamma_2}C_2+\gamma_3^2 e^{-\gamma_3}C_3+\gamma_1^2 e^{\gamma_1}C_4+\gamma_2^2 e^{\gamma_2}C_5+\gamma_3^2 e^{\gamma_3}C_6$$
$$-\lambda_1^2 e^{-\lambda_1}C_7-\lambda_2^2 e^{-\lambda_2}C_8-\lambda_3^2 e^{-\lambda_3}C_9 = 0$$

$$-\gamma_1^3 e^{-\gamma_1}C_1-\gamma_2^3 e^{-\gamma_2}C_2-\gamma_3^3 e^{-\gamma_3}C_3+\gamma_1^3 e^{\gamma_1}C_4+\gamma_2^3 e^{\gamma_2}C_5+\gamma_3^3 e^{\gamma_3}C_6$$
$$+\lambda_1^3 e^{-\lambda_1}C_7+\lambda_2^3 e^{-\lambda_2}C_8+\lambda_3^3 e^{-\lambda_3}C_9 = 0$$

$$\gamma_1^4 e^{-\gamma_1}C_1+\gamma_2^4 e^{-\gamma_2}C_2+\gamma_3^4 e^{-\gamma_3}C_3+\gamma_1^4 e^{\gamma_1}C_4+\gamma_2^4 e^{\gamma_2}C_5+\gamma_3^4 e^{\gamma_3}C_6$$
$$-\lambda_1^4 e^{-\lambda_1}C_7-\lambda_2^4 e^{-\lambda_2}C_8-\lambda_3^4 e^{-\lambda_3}C_9 = 0$$

$$-\gamma_1^5 e^{-\gamma_1} C_1 - \gamma_2^5 e^{-\gamma_2} C_2 - \gamma_3^5 e^{-\gamma_3} C_3 + \gamma_1^5 e^{\gamma_1} C_4 + \gamma_2^5 e^{\gamma_2} C_5 + \gamma_3^5 e^{\gamma_3} C_6$$
$$+ \lambda_1^5 e^{-\lambda_1} C_7 + \lambda_2^5 e^{-\lambda_2} C_8 + \lambda_3^5 e^{-\lambda_3} C_9 = 0$$

where we have written $\beta = 2a^2 + \frac{\sigma}{P}$. The necessary and sufficient condition that the solution given by equations (29) and (30) be non-trivial is that the determinant of the coefficients of the constants in the above equations be zero. That is, we require that the following determinant be zero.

$$\begin{vmatrix} 1 & 1 & 0 \\ -\gamma_i & \gamma_i & 0 \\ \gamma_i^2(\gamma_i^2-\beta) & \gamma_i^2(\gamma_i^2-\beta) & 0 \\ e^{-\gamma_i} & e^{\gamma_i} & -e^{-\lambda_i} \\ -\gamma_i e^{-\gamma_i} & \gamma_i e^{\gamma_i} & \lambda_i e^{-\lambda_i} \\ \gamma_i^2 e^{-\gamma_i} & \gamma_i^2 e^{\gamma_i} & -\lambda_i^2 e^{-\lambda_i} \\ -\gamma_i^3 e^{-\gamma_i} & \gamma_i^3 e^{\gamma_i} & \lambda_i^3 e^{-\lambda_i} \\ \gamma_i^4 e^{-\gamma_i} & \gamma_i^4 e^{\gamma_i} & -\lambda_i^4 e^{-\lambda_i} \\ -\gamma_i^5 e^{-\gamma_i} & \gamma_i^5 e^{\gamma_i} & \lambda_i^5 e^{-\lambda_i} \end{vmatrix} \qquad (45)$$

where each column actually represents three columns corresponding to $i = 1, 2, 3$.

The simplest way of evaluating this determinant analytically is to use Laplace's theorem. This theorem states that if any m rows are selected from a determinant, then the value of the determinant is equal to the sum of the products of all the m^{th} order minors contained in the chosen m rows, each multiplied by its algebraic complement. Let us choose the first three rows of our determinant (45) so that $m = 3$. The number of third order minors contained in the first three rows is 84. However, due to the fact that three of the possible nine rows consist entirely of zeros, only 20 of these minors will have a value which is different from zero. Since these 20 minors are actually 3×3 determinants, a simple analytical evaluation is possible.

The corresponding algebraic complements are 6×6 determinants which can also be evaluated analytically. Taking out the exponential factor appearing in each column of these 6×6 determinants leaves each one in the form

$$\begin{vmatrix} 1 & 1 & 1 & 1 & 1 & 1 \\ x_1 & x_2 & x_3 & x_4 & x_5 & x_6 \\ x_1^2 & x_2^2 & x_3^2 & x_4^2 & x_5^2 & x_6^2 \\ x_1^3 & x_2^3 & x_3^3 & x_4^3 & x_5^3 & x_6^3 \\ x_1^4 & x_2^4 & x_3^4 & x_4^4 & x_5^4 & x_6^4 \\ x_1^5 & x_2^5 & x_3^5 & x_4^5 & x_5^5 & x_6^5 \end{vmatrix}$$

But this is just a Vandermonde determinant which has a known expansion of

$$\prod_{6 \geq i > j \geq 1} (x_i - x_j) \ .$$

That is, the value of the determinant is given by the product of all the differences $(x_i - x_j)$ for which $j<i$.

The method of solution for the eigenvalues is now apparent. Values of the free parameters R, a, and P are first selected. The γ's and λ's, and hence the determinant itself, are then functions of σ only and the value of σ is varied so that the roots of the determinant are located. The values of σ for which the determinant is zero are the desired eigenvalues of the problem. Since we are interested in the largest growth rates, we should pursue only the algebraically largest eigenvalue in each case.

Due to the complicated nature of the expressions for the γ's and for the expansion of the determinant, it is evident that the foregoing procedure leads to a very complicated transcendental equation in σ which will have to be solved numerically for each set of the parameters R, a, and P. It is therefore convenient to evaluate equations (39), (40), and (41) as well as the determinant (45) with the aid of a high-speed digital computer.

When the eigenvalues have been established, the corresponding eigenfunctions can also be determined. To do this, we apply all of the boundary conditions (36), (37), and (38) except one. This enables all of the arbitrary constants, except one, to be determined in terms of the one remaining undetermined constant. In this way, dropping the last boundary condition of equation (36) and taking C_9 as the arbitrary constant, we obtain the following system of equations to be solved.

$$
\begin{pmatrix}
1 & 1 & 1 & 1 & 1 & 1 & 0 & 0 \\
-\gamma_1 & -\gamma_2 & -\gamma_3 & \gamma_1 & \gamma_2 & \gamma_3 & 0 & 0 \\
e^{-\gamma_1} & e^{-\gamma_2} & e^{-\gamma_3} & e^{\gamma_1} & e^{\gamma_2} & e^{\gamma_3} & -e^{-\lambda_1} & -e^{-\lambda_2} \\
-\gamma_1 e^{-\gamma_1} & -\gamma_2 e^{-\gamma_2} & -\gamma_3 e^{-\gamma_3} & \gamma_1 e^{\gamma_1} & \gamma_2 e^{\gamma_2} & \gamma_3 e^{\gamma_3} & \lambda_1 e^{-\lambda_1} & \lambda_2 e^{-\lambda_2} \\
\gamma_1^2 e^{-\gamma_1} & \gamma_2^2 e^{-\gamma_2} & \gamma_3^2 e^{-\gamma_3} & \gamma_1^2 e^{\gamma_1} & \gamma_2^2 e^{\gamma_2} & \gamma_3^2 e^{\gamma_3} & -\lambda_1^2 e^{-\lambda_1} & -\lambda_2^2 e^{-\lambda_2} \\
-\gamma_1^3 e^{-\gamma_1} & -\gamma_2^3 e^{-\gamma_2} & -\gamma_3^3 e^{-\gamma_3} & \gamma_1^3 e^{\gamma_1} & \gamma_2^3 e^{\gamma_2} & \gamma_3^3 e^{\gamma_3} & \lambda_1^3 e^{-\lambda_1} & \lambda_2^3 e^{-\lambda_2} \\
\gamma_1^4 e^{-\gamma_1} & \gamma_2^4 e^{-\gamma_2} & \gamma_3^4 e^{-\gamma_3} & \gamma_1^4 e^{\gamma_1} & \gamma_2^4 e^{\gamma_2} & \gamma_3^4 e^{\gamma_3} & -\lambda_1^4 e^{-\lambda_1} & -\lambda_2^4 e^{-\lambda_2} \\
-\gamma_1^5 e^{-\gamma_1} & -\gamma_2^5 e^{-\gamma_2} & -\gamma_3^5 e^{-\gamma_3} & \gamma_1^5 e^{\gamma_1} & \gamma_2^5 e^{\gamma_2} & \gamma_3^5 e^{\gamma_3} & \lambda_1^5 e^{-\lambda_1} & \lambda_2^5 e^{-\lambda_2}
\end{pmatrix}
\begin{pmatrix} C_1 \\ C_2 \\ C_3 \\ C_4 \\ C_5 \\ C_6 \\ C_7 \\ C_8 \end{pmatrix}
=
\begin{pmatrix} 0 \\ 0 \\ e^{-\lambda_3} \\ -\lambda_3 e^{-\lambda_3} \\ \lambda_3^2 e^{-\lambda_3} \\ -\lambda_3^3 e^{-\lambda_3} \\ \lambda_3^4 e^{-\lambda_3} \\ -\lambda_3^5 e^{-\lambda_3} \end{pmatrix}
\qquad C_9
$$

This system can be solved for C_1/C_9 , C_2/C_9 , ... , C_8/C_9 , after which the velocity and temperature can be found from the relations

$$W_1 = C_9\left(\frac{C_1}{C_9}e^{-\gamma_1 z}+\frac{C_2}{C_9}e^{-\gamma_2 z}+\frac{C_3}{C_9}e^{-\gamma_3 z}+\frac{C_4}{C_9}e^{\gamma_1 z}+\frac{C_5}{C_9}e^{\gamma_2 z}+\frac{C_6}{C_9}e^{\gamma_3 z}\right) \tag{46}$$

$$W_2 = C_9\left(\frac{C_7}{C_9}e^{-\lambda_1 z}+\frac{C_8}{C_9}e^{-\lambda_2 z}+e^{-\lambda_3 z}\right) \tag{47}$$

$$T_1 = \frac{C_9}{a^2}\left[\frac{C_1}{C_9}(\gamma_1^4-\beta\gamma_1^2+\tau)e^{-\gamma_1 z}+\frac{C_2}{C_9}(\gamma_2^4-\beta\gamma_2^2+\tau)e^{-\gamma_2 z}+\frac{C_3}{C_9}(\gamma_3^4-\beta\gamma_3^2+\tau)e^{-\gamma_3 z}\right.$$
$$\left.+\frac{C_4}{C_9}(\gamma_1^4-\beta\gamma_1^2+\tau)e^{\gamma_1 z}+\frac{C_5}{C_9}(\gamma_2^4-\beta\gamma_2^2+\tau)e^{\gamma_2 z}+\frac{C_6}{C_9}(\gamma_3^4-\beta\gamma_3^2+\tau)e^{\gamma_3 z}\right] \tag{48}$$

$$T_2 = \frac{C_9}{a^2}\left[\frac{C_7}{C_9}(\lambda_1^4-\beta\lambda_1^2+\tau)e^{-\lambda_1 z}+\frac{C_8}{C_9}(\lambda_2^4-\beta\lambda_2^2+\tau)e^{-\lambda_2 z}+(\lambda_3^4-\beta\lambda_3^2+\tau)e^{-\lambda_3 z}\right] \tag{49}$$

where we have set $\tau = a^2\left(a^2+\frac{\sigma}{P}\right)$. The constant C_9 , and hence the amplitude of the perturbations, is undetermined in the linear theory.

7. Marginal Stability

In comparing the analytical results with the published experimental results, the critical Rayleigh number for a finite fluid having a non-linear temperature profile will be required. Furthermore, the results for the semi-infinite fluid may be obtained from the results for a finite fluid by taking an appropriate limit, as we will show in a later section. For these reasons, the critical Rayleigh number will be calculated for the case of a finite fluid layer.

By critical Rayleigh number, we mean the numerically smallest value of R for which all the Fourier components of an arbitrary disturbance are decaying, except one. This particular wave component is the fastest growing, and in the critical state it is marginally stable. That is, it is neither growing nor decaying. The disturbance corresponding to this wave number must satisfy equation (20) but, since the motion is steady, we set $\partial/\partial t = 0$. Then the stability equation becomes

$$\left(\frac{\partial^2}{\partial z^2} - a^2\right)^3 w = a^2 \frac{\partial T^{(o)}}{\partial z} w \ . \tag{50}$$

By considering only short time intervals and replacing the continuous conduction temperature profile by two straight line segments, as before, we obtain the following two ordinary differential equations:

$$\left(D^2-a^2\right)^3 W_1 = -a^2 R W_1 \ , \tag{51}$$

$$\left(D^2-a^2\right)^3 W_2 = 0 \ . \tag{52}$$

The general solutions to equations (51) and (52) are

$$W_1 = C_1 e^{-\gamma_1 z} + C_2 e^{-\gamma_2 z} + C_3 e^{-\gamma_3 z} + C_4 e^{\gamma_1 z} + C_5 e^{\gamma_2 z} + C_6 e^{\gamma_3 z} \tag{53}$$

$$W_2 = (C_7+C_8z+C_9z^2)e^{-az} + (C_{10}+C_{11}z+C_{12}z^2)e^{az} \tag{54}$$

where the γ's are given by

$$\gamma_1 = a\left[1 - \left(\frac{R}{4a}\right)^{1/3}\right]^{1/2} \tag{55}$$

$$\gamma_2 = a\left[1 + \frac{1}{2}\left(1+i\sqrt{3}\right)\left(\frac{R}{4a}\right)^{1/3}\right]^{1/2} \tag{56}$$

$$\gamma_3 = a\left[1 + \frac{1}{2}\left(1-i\sqrt{3}\right)\left(\frac{R}{4a}\right)^{1/3}\right]^{1/2} \tag{57}$$

The boundary conditions must now be applied on the planes $z = 0$, 1, and ζ, where ζ is the non-dimensional thickness of the fluid layer. The boundary conditions on $z = 0$ and $z = 1$ will be as before, and the boundary conditions on the upper surface at $z = \zeta$ will be the same as those on the lower surface at $z = 0$.

On $z = 0$;

$$W_1 = DW_1 = D^2(D^2-2a^2)W_1 = 0 \tag{58}$$

On $z = 1$;

$$(W_1-W_2) = (D^nW_1-D^nW_2) = 0 \qquad n = 1, 2, 3, 4, 5 \tag{59}$$

On $z = \zeta$;

$$W_2 = DW_2 = D^2(D^2-2a^2)W_2 = 0 \tag{60}$$

The solution (53) and (54), together with the boundary conditions (58), (59), and (60), yield a set of twelve homogeneous algebraic equations in the twelve arbitrary constants. The requirement that these equations have a non-trivial solution leads to the condition that the determinant of the coefficients of the arbitrary constants be zero. That is, the following determinant must be zero.

$$
\begin{vmatrix}
1 & 1 & 0 & 0 & 0 & 0 & 0 & 0 \\
-\gamma_i & \gamma_i & 0 & 0 & 0 & 0 & 0 & 0 \\
\gamma_i^2(\gamma_i^2-2a^2) & \gamma_i^2(\gamma_i^2-2a^2) & 0 & 0 & 0 & 0 & 0 & 0 \\
e^{-\gamma_i} & e^{-\gamma_i} & -e^{-a} & -e^{-a} & -e^{-a} & -e^{a} & -e^{a} & -e^{a} \\
-\gamma_i e^{-\gamma_i} & \gamma_i e^{\gamma_i} & ae^{-a} & -(1-a)e^{-a} & -(2-a)e^{-a} & -ae^{a} & -(1+a)e^{a} & -(2+a)e^{a} \\
\gamma_i^2 e^{-\gamma_i} & \gamma_i^2 e^{\gamma_i} & -a^2e^{-a} & a(2-a)e^{-a} & -(2-4a+a^2)e^{-a} & -a^2e^{a} & -a(2+a)e^{a} & -(2+4a+a^2)e^{a} \\
-\gamma_i^3 e^{-\gamma_i} & \gamma_i^3 e^{\gamma_i} & a^3e^{-a} & -a^2(3-a)e^{-a} & a(6-6a+a^2)e^{-a} & -a^3e^{a} & -a^2(3+a)e^{a} & -a(6+6a+a^2)e^{a} \\
\gamma_i^4 e^{-\gamma_i} & \gamma_i^4 e^{\gamma_i} & -a^4e^{-a} & a^3(4-a)e^{-a} & -a^2(12-8a+a^2)e^{-a} & -a^4e^{a} & -a^3(4+a)e^{a} & -a^2(12+8a+a^2)e^{a} \\
-\gamma_i^5 e^{-\gamma_i} & \gamma_i^5 e^{\gamma_i} & a^5e^{-a} & -a^4(5-a)e^{-a} & a^3(20-10a+a^2)e^{-a} & -a^5e^{a} & -a^4(5+a)e^{a} & -a^3(20+10a+a^2)e^{a} \\
0 & 0 & e^{-a\zeta} & \zeta e^{-a\zeta} & \zeta^2e^{-a\zeta} & e^{a\zeta} & \zeta e^{a\zeta} & \zeta^2e^{a\zeta} \\
0 & 0 & -ae^{-a\zeta} & (1-a\zeta)e^{-a\zeta} & (2\zeta-a\zeta^2)e^{-a\zeta} & ae^{a\zeta} & (1+a\zeta)e^{a\zeta} & (2\zeta+a\zeta^2)e^{a\zeta} \\
0 & 0 & -a^4e^{-a\zeta} & -a^4\zeta e^{-a\zeta} & -a^2(a^2\zeta^2-8)e^{-a\zeta} & -a^4e^{a\zeta} & -a^4\zeta e^{a\zeta} & -a^2(a^2\zeta^2-8)e^{a\zeta}
\end{vmatrix}
\tag{61}
$$

The first two columns of (61) each represent three columns, corresponding to the three values of γ given by equations (55), (56), and (57).

The eigenvalues here are values of the Rayleigh number and they are obtained by iteration. For given values of the wave number a and the thickness ζ, we must vary the value of R until the determinant (61) is zero.

III. RESULTS AND DISCUSSION

1. Behavior of Determinant

Before discussing the nature of the numerical results, two special roots of the determinant (45) should be examined. The first of these special roots comes about through coalescing of two of the γ's. In this case, two pairs of columns of the determinant (45) will be identical so that its numerical value will be zero. Equations (40) and (41) show that γ_2 will be equal to γ_3 if A = B. From the definitions of A and B we see that this will occur when

$$\left[\frac{1}{4}a^4R^2 - \frac{a^2R}{54}\left(1+\frac{1}{P}\right)\left(2-\frac{1}{P}\right)\left(1-\frac{2}{P}\right)\sigma^3 - \frac{1}{108P^2}\left(1-\frac{1}{P}\right)^2\sigma^6\right]^{\frac{1}{2}} = 0 .$$

Squaring and solving the quadratic equation for σ^3, we find that the values of σ which create this condition are given by

$$\sigma = a^{\frac{2}{3}}R^{\frac{1}{3}}\left\{\frac{P^2\left(1+\frac{1}{P}\right)\left(2-\frac{1}{P}\right)\left(1-\frac{2}{P}\right)}{\left(1-\frac{1}{P}\right)^2}\left[+\sqrt{1+\frac{27\left(1-\frac{1}{P}\right)^2}{P^2\left(1+\frac{1}{P}\right)^2\left(2-\frac{1}{P}\right)^2\left(1-\frac{2}{P}\right)^2}} - 1\right]\right\}^{\frac{1}{3}}$$

For $\frac{1}{2} < P < 2$ the positive value of σ so defined is associated with the negative square root and may be expressed in the form

$$\sigma_1 = a^{\frac{2}{3}}R^{\frac{1}{3}}\left\{\frac{P(P+1)(2P-1)(2-P)}{(P-1)^2}\left[\sqrt{1+\frac{27P^2(P-1)^2}{(P+1)^2(2P-1)^2(2-P)^2}} + 1\right]\right\}^{\frac{1}{3}} \tag{62}$$

Here we have used σ_1 to distinguish this particular value of σ. For a given Prandtl number, σ_1 is a simple function of a and R.

Although σ_1 is a root of the determinant (45), it is not a true eigenvalue of our problem. This is due to the fact that the solution (29) was written down under the assumption of distinct γ's. For

$\gamma_2 = \gamma_3$, the solution takes the form

$$W_1 = C_1 e^{-\gamma_1 z} + (C_2 + C_3 z) e^{-\gamma_2 z} + C_4 e^{\gamma_1 z} + (C_5 + C_6 z) e^{\gamma_2 z} .$$

The corresponding determinant is not zero when $\sigma = \sigma_1$ so that σ_1 is not a true eigenvalue.

For σ real and less than σ_1 , both γ_2 and γ_3 will be complex; while for σ greater than σ_1 , γ_2 and γ_3 will be real. γ_1^2 will always be real but, since γ_1^2 may be negative, γ_1 itself may be imaginary. The transition from γ_1 being real to its becoming imaginary will correspond to γ_1 being zero. The simplest method of finding the corresponding values of σ is to observe that the general solution, when γ_1 is zero, is of the form

$$W_1 = (C_1 + C_4 z) + C_2 e^{-\gamma_2 z} + C_3 e^{-\gamma_3 z} + C_5 e^{\gamma_2 z} + C_6 e^{\gamma_3 z} . \qquad (63)$$

Now if this solution is to satisfy the boundary conditions, the constant C_1 must not be zero. On the other hand, if $W_1 = C_1$ is to be a solution of the differential equation (25), then the coefficient of W_1 itself in that equation must be zero. That is, we must have

$$-a^2(a^2+\sigma)\left(a^2+\frac{\sigma}{P}\right) = -a^2 R .$$

This is a quadratic equation in σ which has the solutions

$$\sigma = \frac{a^2}{2}(P+1)\left\{ \begin{matrix} + \\ - \end{matrix} \sqrt{1 + \frac{4P}{(P+1)^2}\left(\frac{R}{a^4} - 1\right)} - 1 \right\} . \qquad (64)$$

As $a \to 0$, $\sigma_o \to PR$, and σ_o is zero when $a^4 = R$. As we have pointed out, the solution for W_1 when γ_1 is zero is given by equation (63) rather than equation (29). Applying the boundary conditions to equation (63) shows that σ_o is not a true eigenvalue.

Apart from σ_o and σ_1 and the corresponding negative values, which are all functions of the free parameters R, a, and P, there is a fixed root of the determinant (45) at $\sigma = 0$. In this case, equations (43) and (44) show that λ_2 and λ_3 coalesce. Again, the exact solution shows that $\sigma = 0$ is not a true eigenvalue, at least for arbitrary values of the free parameters.

Although the values of σ mentioned above are not true eigenvalues, it is useful to locate these roots of the determinant. In particular, σ_o and σ_1 are most useful, since they play important roles in the behavior of the determinant in the vicinity of the largest eigenvalue.

Since the determinant is in general complex, it might appear that in order to get both the real and the imaginary parts to vanish simultaneously we would require two parameters. That is, it might be supposed that σ is complex and that both the real and imaginary parts of σ have to be adjusted in order to reduce the determinant to zero. However, it is found that roots of the determinant (45) can be found by considering σ to be real. This means that the principle of the exchange of stabilities is valid here also, as in the case of a uniform density stratification, but it is presented here as a numerical observation only, for which an analytical proof has not yet been found. The fact that σ is real means that disturbances will grow aperiodically in time, which is in accord with physical observations.

Typical behavior of the determinant is shown in Figure 3. For $\sigma > \sigma_o > \sigma_1$, all of the γ's are real and, since the λ's are always real, the determinant itself is real. For $\sigma < \sigma_1 < \sigma_o$, γ_1 *is imagi-*

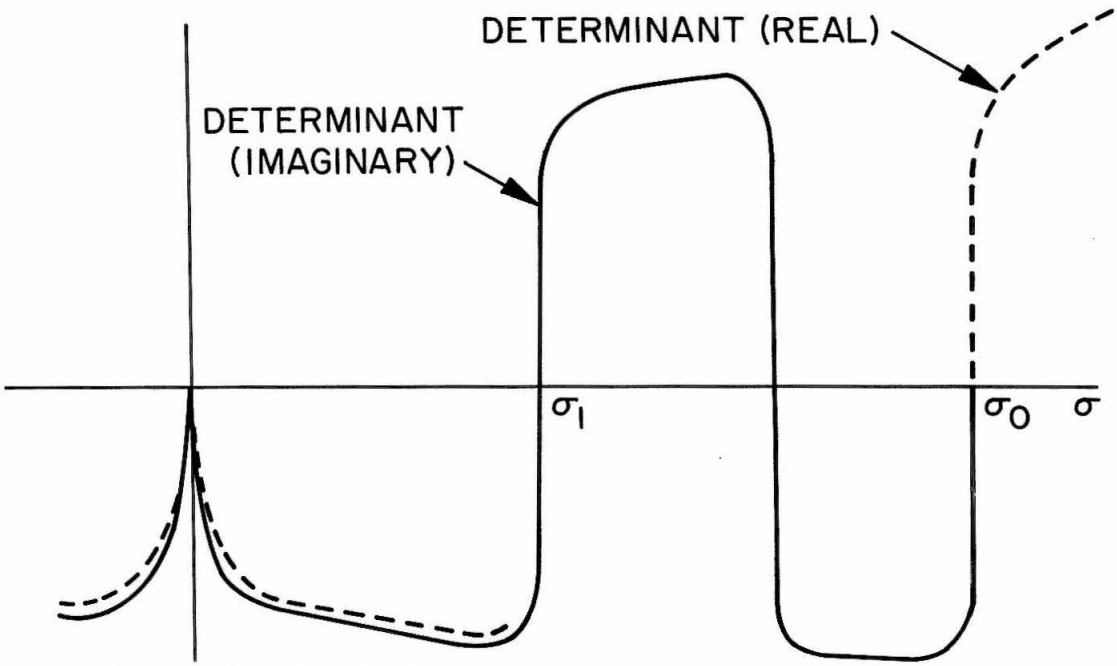

(a) ROOT IN RANGE $\sigma_1 < \sigma < \sigma_0$

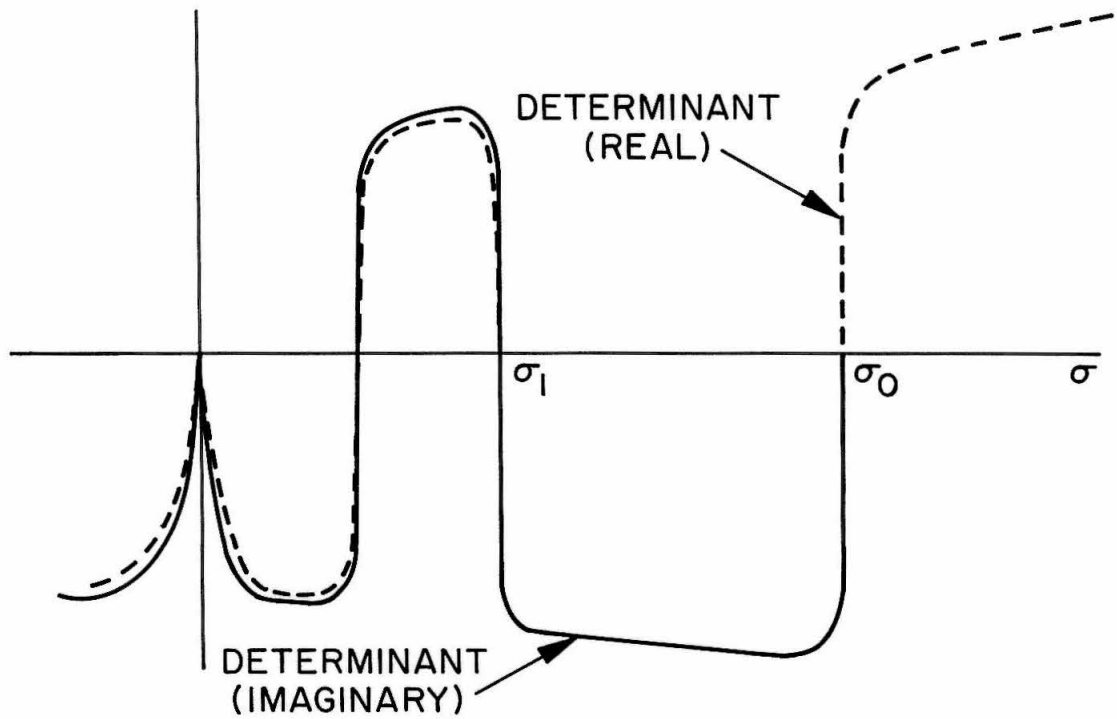

(b) ROOT IN RANGE $\sigma < \sigma < \sigma_1$

FIGURE 3 – BEHAVIOUR OF DETERMINANT

nary, while both γ_2 and γ_3 are complex. In this case, the determinant is complex, but both the real and imaginary parts vanish for the same values of σ. For $\sigma_1 < \sigma < \sigma_o$, the determinant is purely imaginary. Since γ_2 and γ_3 as well as all the λ's are real, the imaginary nature must come from γ_1. We have already shown that in this range γ_1 is pure imaginary, so that, writing $\gamma_1 = i\bar{\gamma}_1$, columns one and four of the determinant (45) become, respectively,

$1 + i\,0$	$1 + i\,0$
$0 - i\,\bar{\gamma}_1$	$0 + i\,\bar{\gamma}_1$
$\bar{\gamma}_1^2(\bar{\gamma}_1^2+\beta) + i\,0$	$\bar{\gamma}_1^2(\bar{\gamma}_1^2+\beta) + i\,0$
$\cos\bar{\gamma}_1 - i\sin\bar{\gamma}_1$	$\cos\bar{\gamma}_1 + i\sin\bar{\gamma}_1$
$-\bar{\gamma}_1\sin\bar{\gamma}_1 - i\,\bar{\gamma}_1\cos\bar{\gamma}_1$	$-\bar{\gamma}_1\sin\bar{\gamma}_1 + i\,\bar{\gamma}_1\cos\bar{\gamma}_1$
$-\bar{\gamma}_1^2\cos\bar{\gamma}_1 + i\,\bar{\gamma}_1^2\sin\bar{\gamma}_1$	$-\bar{\gamma}_1^2\cos\bar{\gamma}_1 - i\,\bar{\gamma}_1^2\sin\bar{\gamma}_1$
$\bar{\gamma}_1^3\sin\bar{\gamma}_1 + i\,\bar{\gamma}_1^3\cos\bar{\gamma}_1$	$\bar{\gamma}_1^3\sin\bar{\gamma}_1 - i\,\bar{\gamma}_1^3\cos\bar{\gamma}_1$
$\bar{\gamma}_1^4\cos\bar{\gamma}_1 - i\,\bar{\gamma}_1^4\sin\bar{\gamma}_1$	$\bar{\gamma}_1^4\cos\bar{\gamma}_1 + i\,\bar{\gamma}_1^4\sin\bar{\gamma}_1$
$-\bar{\gamma}_1^5\sin\bar{\gamma}_1 - i\,\bar{\gamma}_1^5\cos\bar{\gamma}_1$	$-\bar{\gamma}_1^5\sin\bar{\gamma}_1 + i\,\bar{\gamma}_1^5\cos\bar{\gamma}_1$

All of the other columns will have real elements only. Now the determinant (45) can be expressed as the sum of four determinants. In the first of these four determinants we enter only the real parts of columns one and four. Since these real parts are identical, this determinant will have two identical columns, and so its numerical value will be zero. In the second determinant we enter only the imaginary parts of columns one and four. Since these parts are numerically

equal, this determinant will also be zero. The remaining two determinents will contain the real part of column one with the imaginary part of column four, and vice versa. These two determinants are numerically the same and they will add, since one will look just like the other but with two of the rows interchanged and one of these rows multiplied by -1. The factor -1 comes about since the imaginary parts of columns one and four are opposite in sign. The factor $i = \sqrt{-1}$ may now be taken outside of this non-zero determinant leaving it with real elements. Hence the determinant (45) will be pure imaginary.

For values of σ less than σ_1, the real and imaginary parts of the determinant are of the same order and are in phase with one another as shown in Figure 3.

2. Growth Rates of Disturbances

The eigenvalues corresponding to the largest growth rates have been established for Rayleigh numbers of 10^3, 10^4, and 10^5 for Prandtl numbers of 7.0 and 0.7. The selected Prandtl numbers correspond closely to water and air at ambient temperature.

The results for $R = 10^5$ and $P = 7.0$ are shown in Figure 4. It is seen that a large portion of this curve falls in the region $\sigma_1 < \sigma < \sigma_o$ and that σ approaches σ_o as σ_o tends to zero.

Figure 5 shows the results for $R = 10^4$ and $P = 7.0$. Here, a much smaller portion of the curve falls in the range $\sigma_1 < \sigma < \sigma_o$, but σ still tends to σ_o as they both become small.

For $R = 10^3$ and $P = 7.0$, Figure 6 shows that the growth rate curve lies entirely below σ_1 as well as σ_o. From this and the previous curves we conclude that the effect of increasing the Rayleigh number is to increase the growth rate of disturbances and the wave number at which the maximum growth rate occurs. Furthermore, the spectrum of wavelengths for which infinitesimal disturbances become unstable is increased for the higher Rayleigh numbers.

Results for the same three Rayleigh numbers but for a Prandtl number of 0.7 are shown in Figures 7, 8, and 9. These curves differ from the previous ones in so much as the solution curve σ never exceeds the curve σ_1. However, σ_o is still an upper bound and as before σ and σ_o tend to coalesce as they approach zero.

The solution curves themselves are shown in Figure 10 where they are all drawn to the same scale for comparison.

Since positive growth rates have been obtained for a Rayleigh

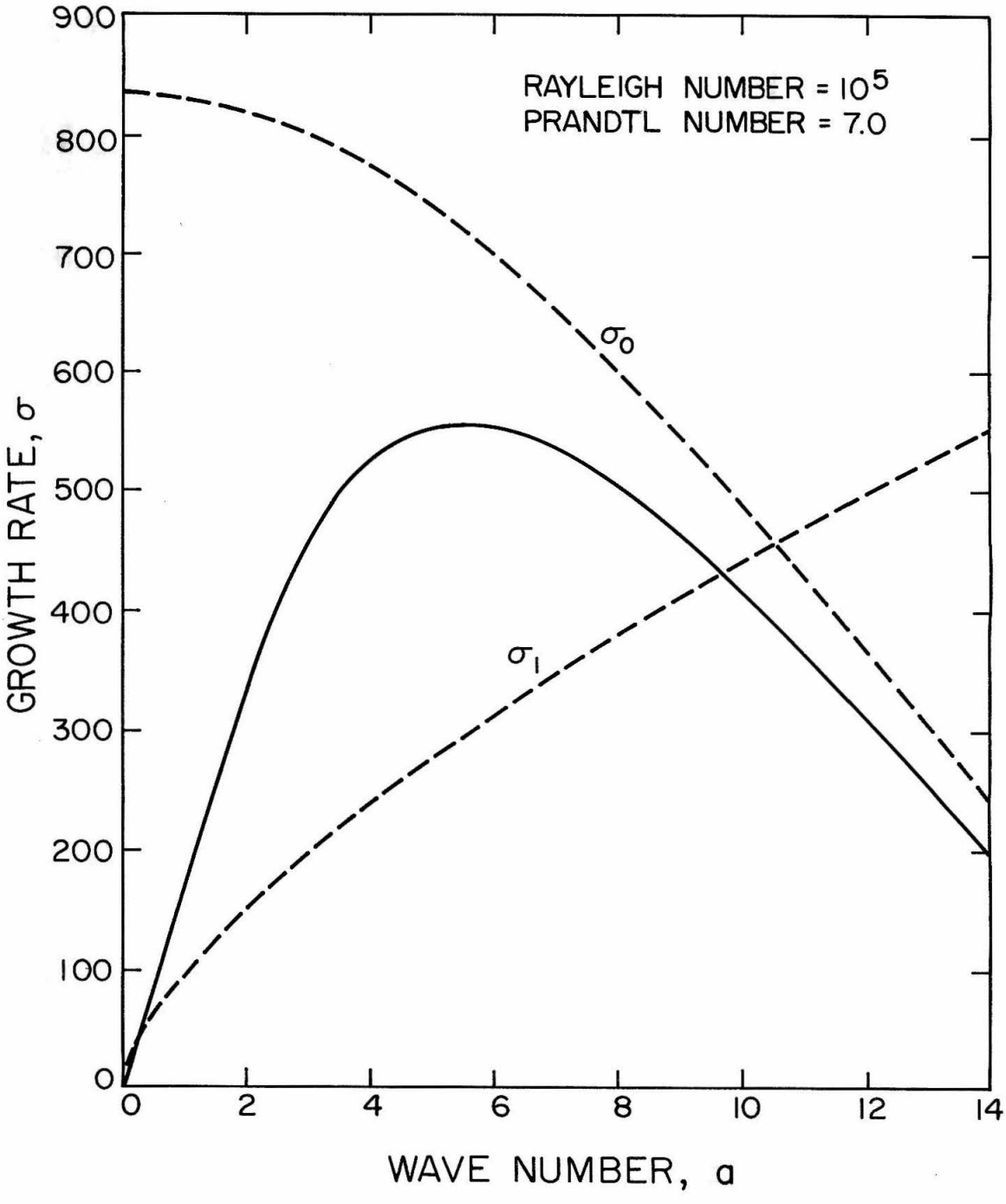

FIGURE 4 - GROWTH RATE OF DISTURBANCES

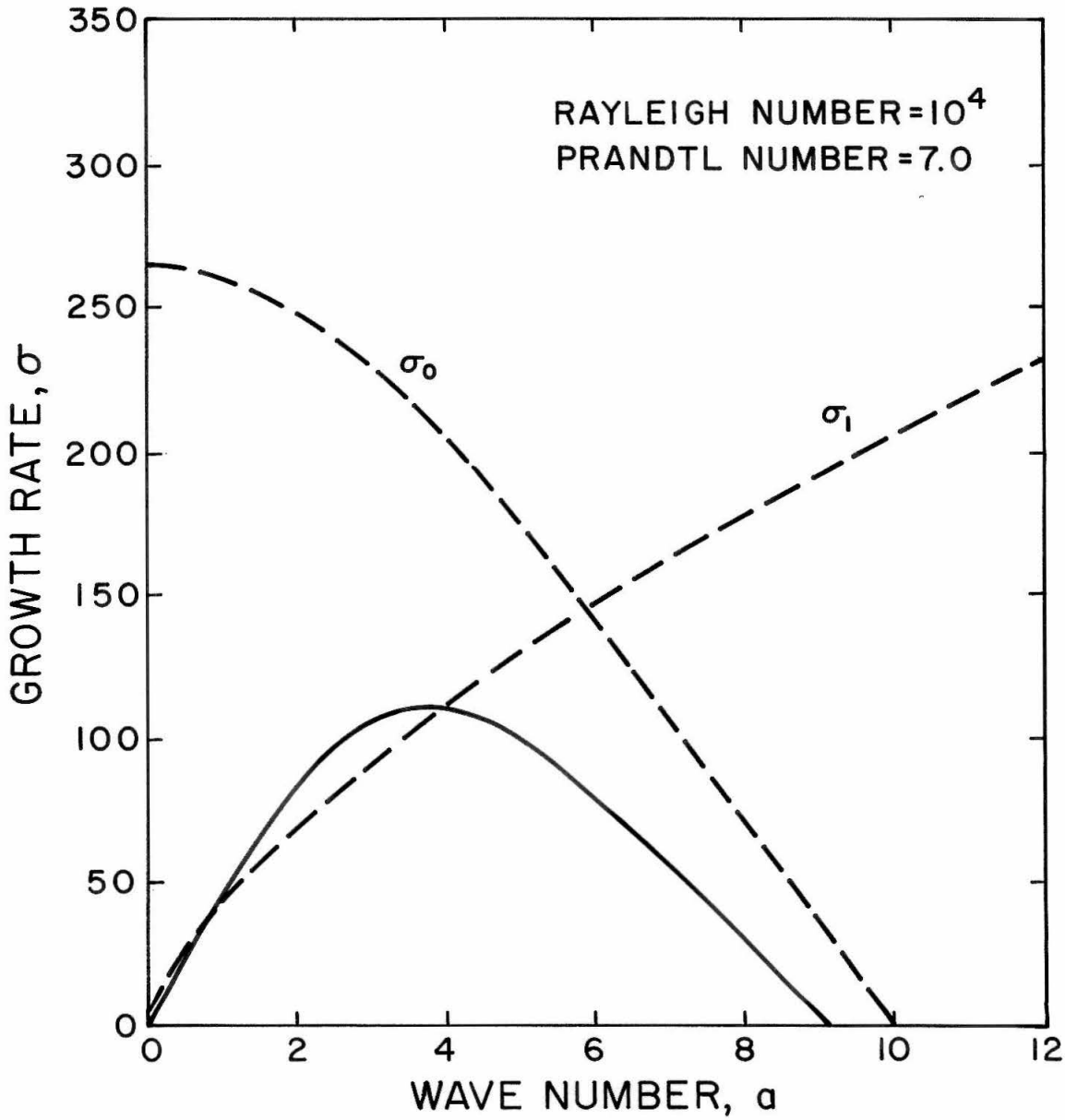

FIGURE 5 - GROWTH RATE OF DISTURBANCES

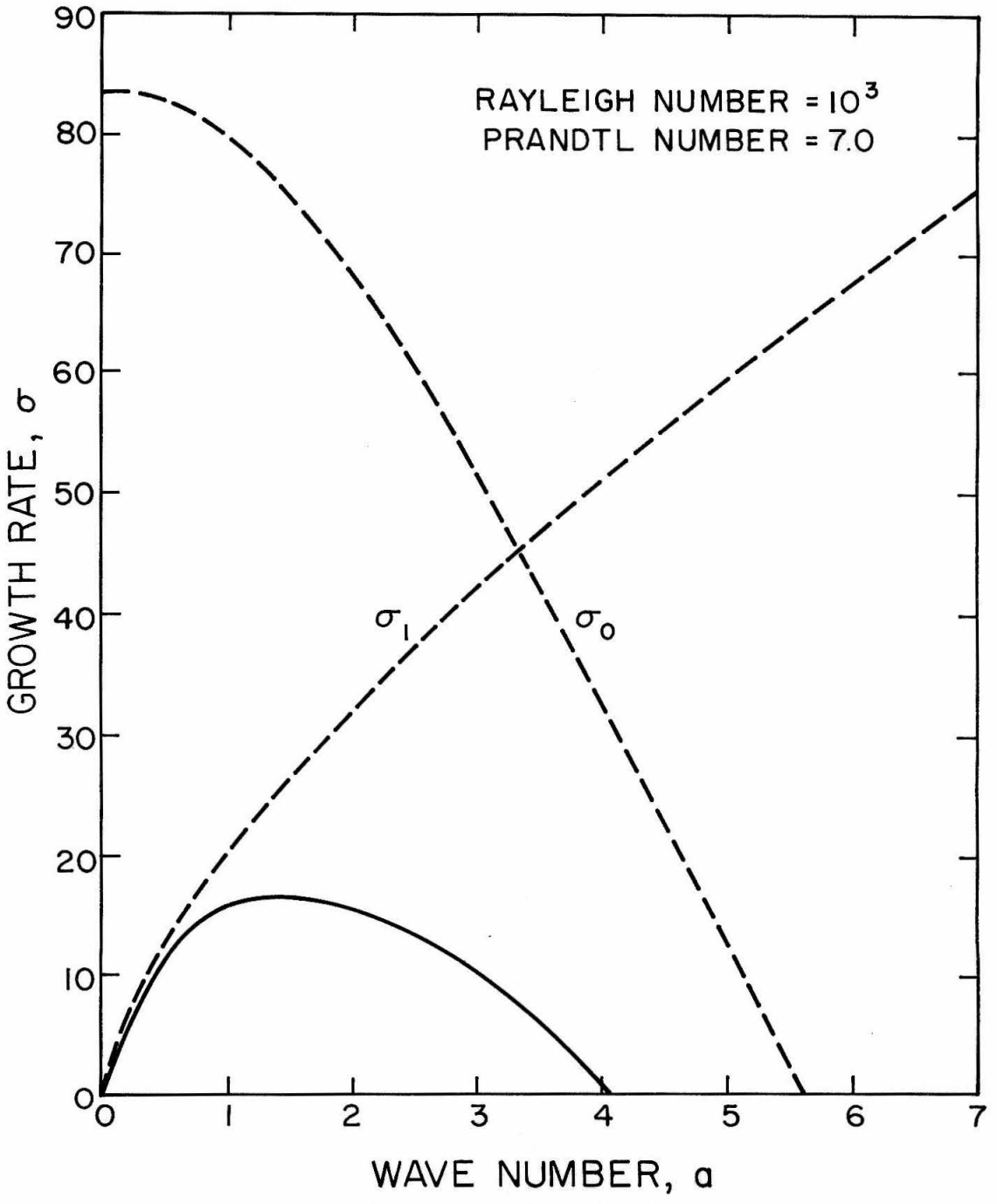

FIGURE 6 – GROWTH RATE OF DISTURBANCES

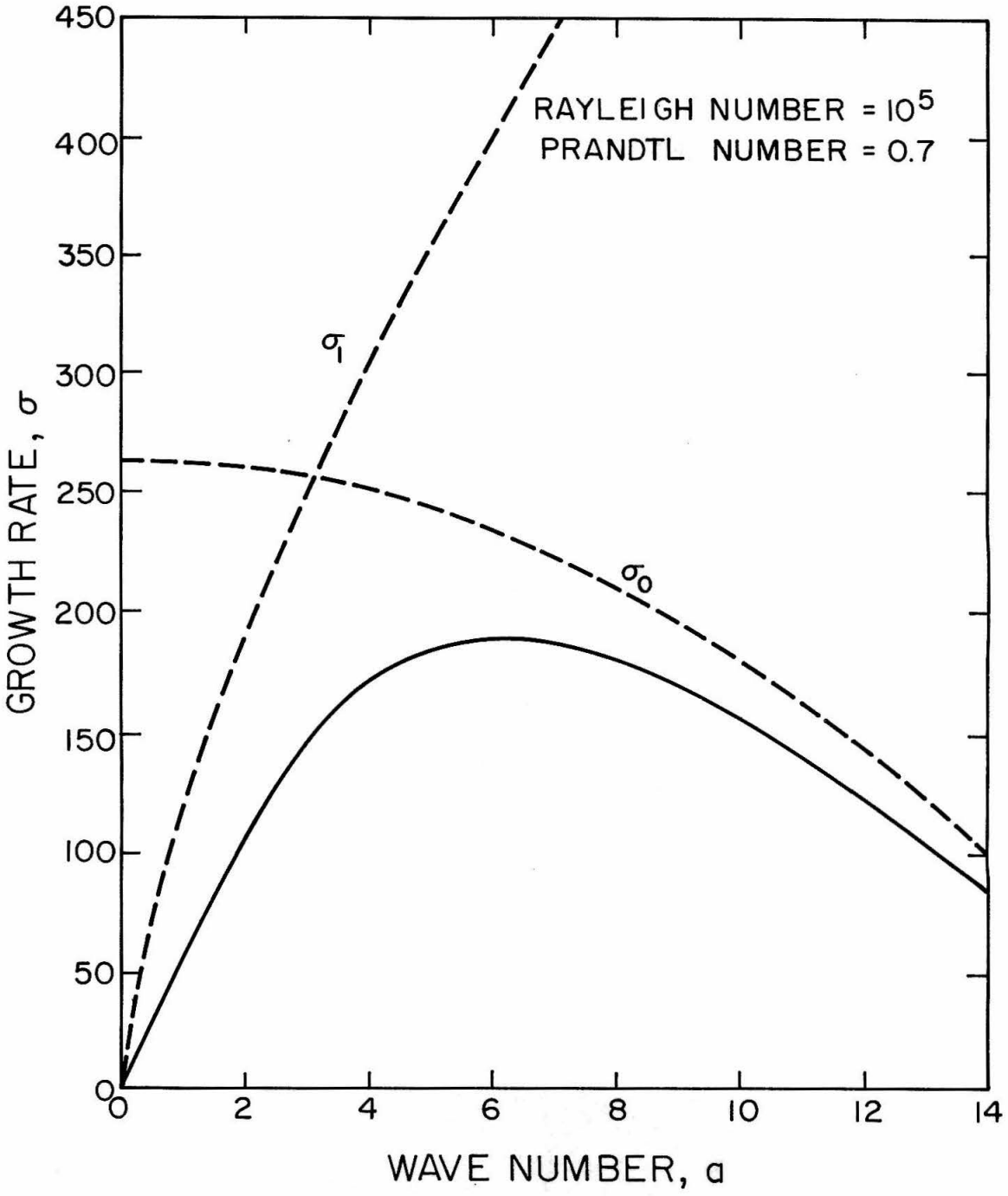

FIGURE 7 – GROWTH RATE OF DISTURBANCES

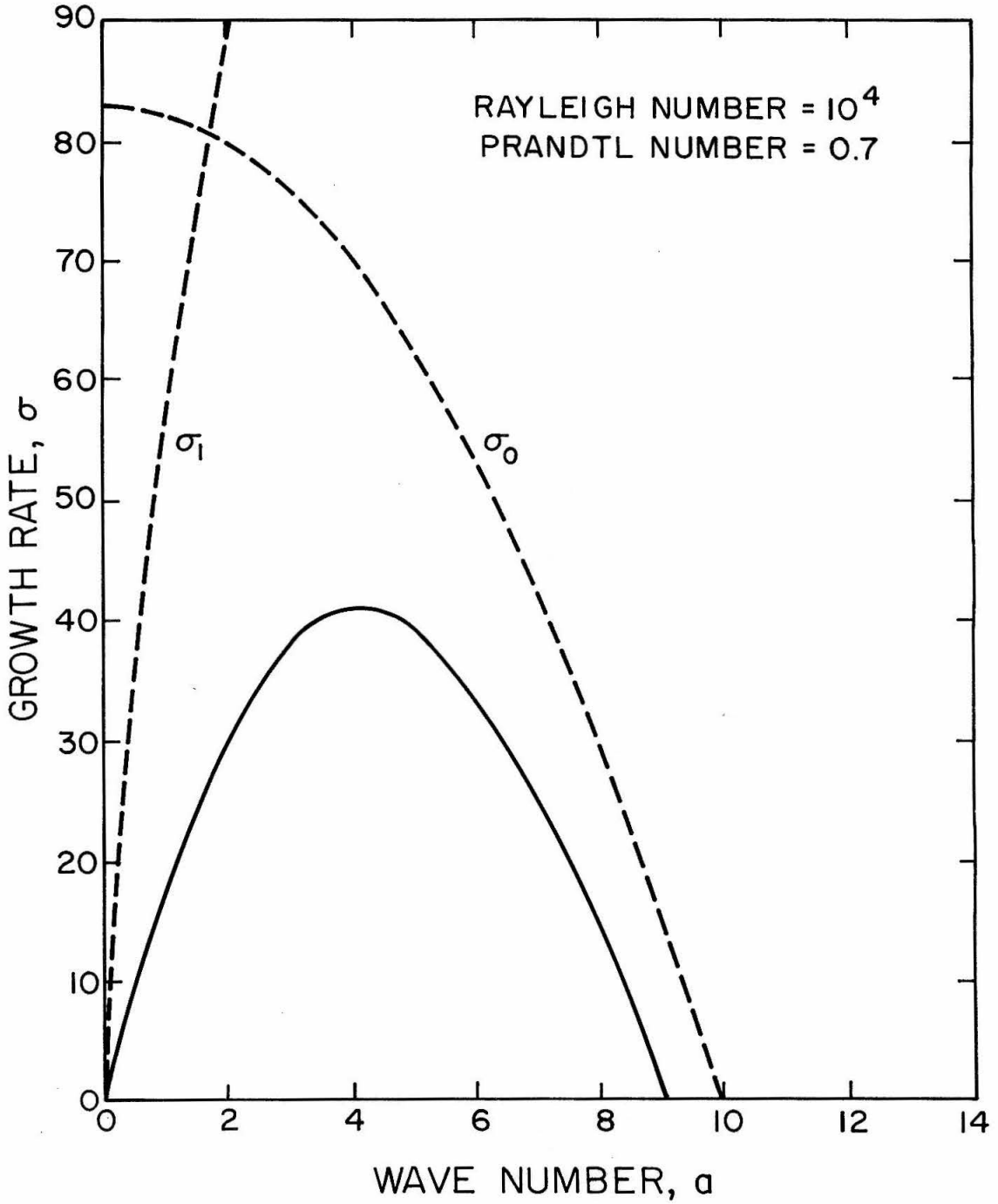

FIGURE 8 – GROWTH RATE OF DISTURBANCES

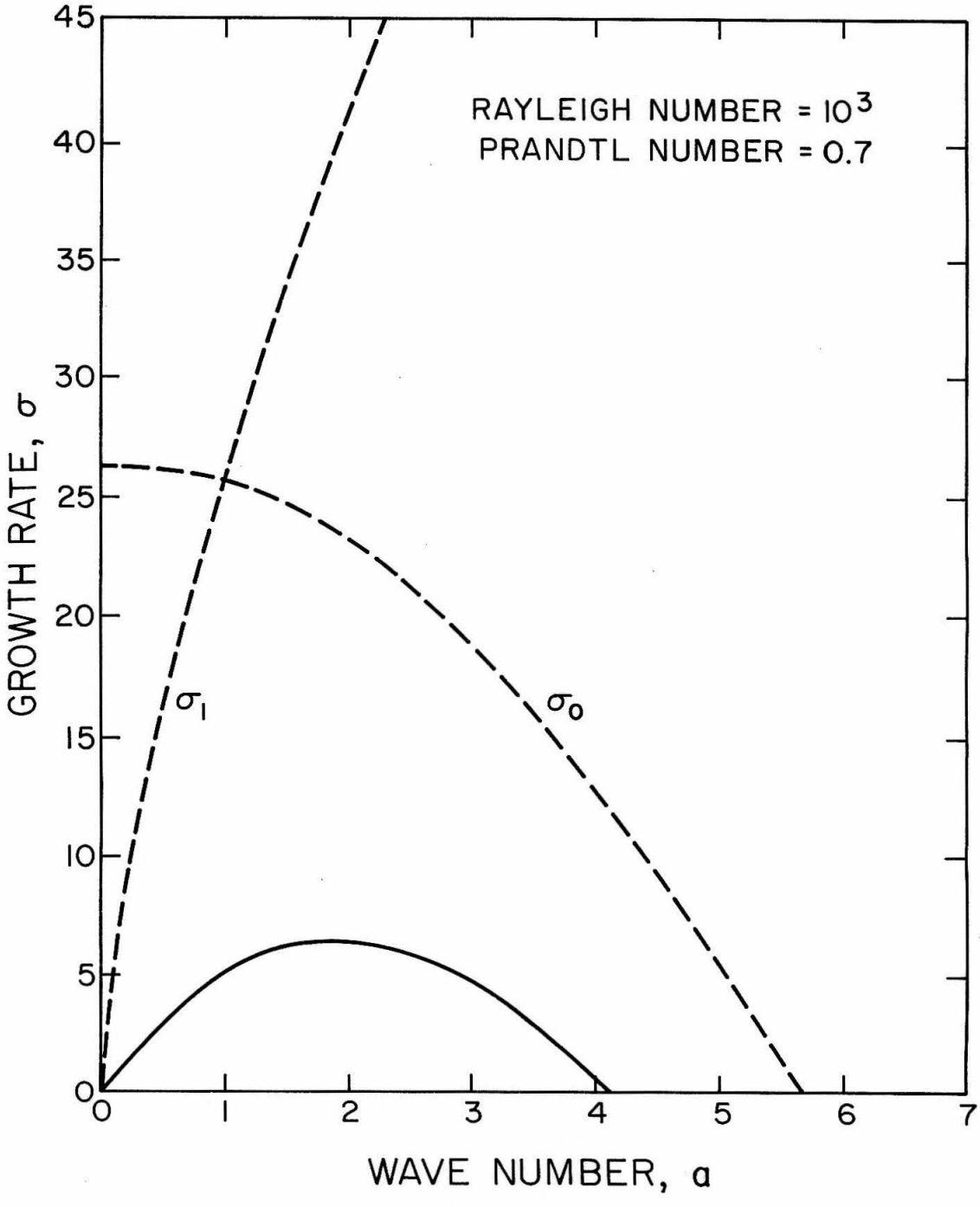

FIGURE 9 — GROWTH RATE OF DISTURBANCES

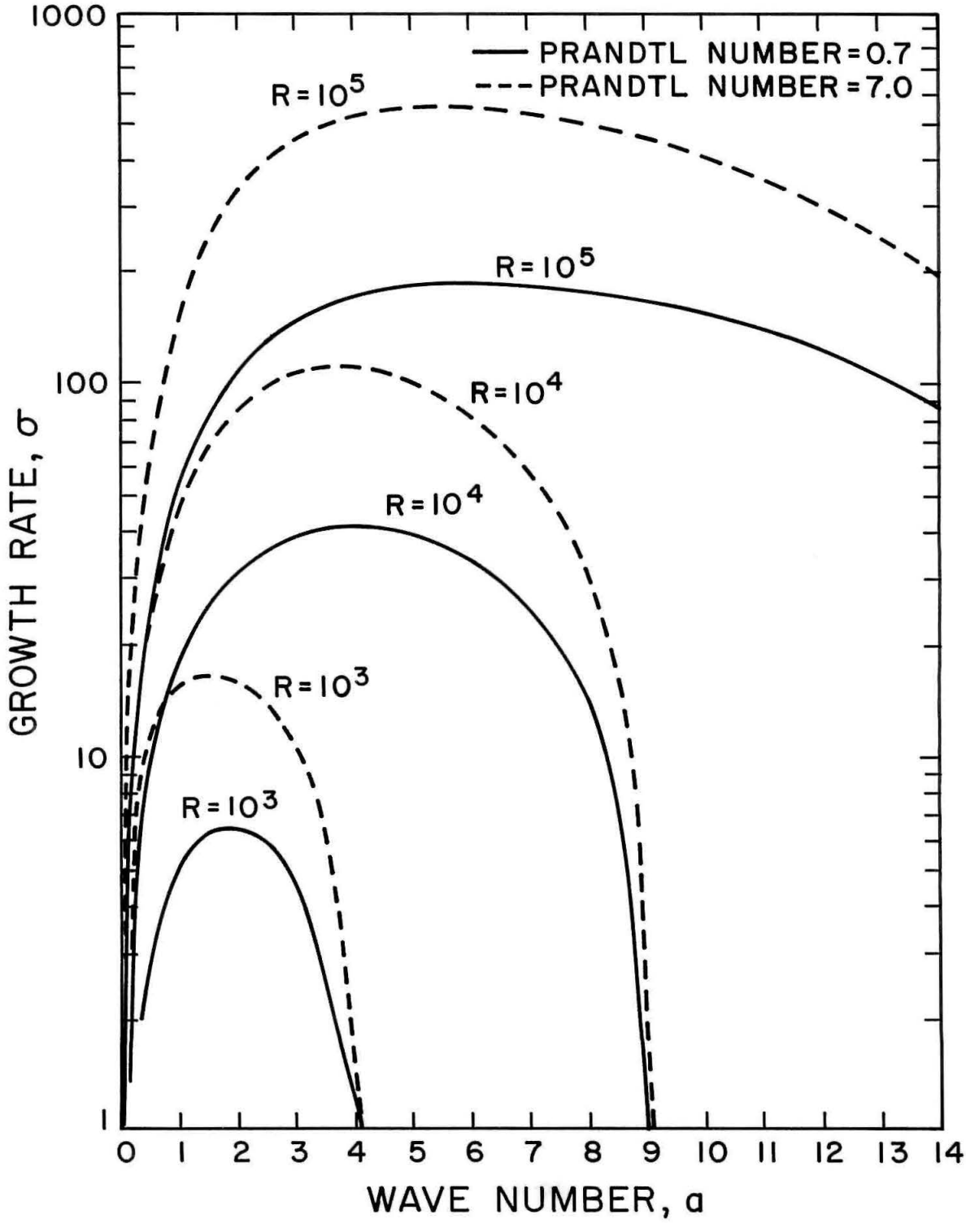

FIGURE 10 - GROWTH RATE OF DISTURBANCES

number of 10^3 and for both Prandtl numbers, it is evident that the stability of the sub-layer with the non-zero temperature gradient has been decreased. The critical Rayleigh number for a fluid layer with a rigid boundary below and a free boundary above is 1100. The effect of the interface with the upper region of fluid causes two modifications over the free surface case. First of all, the perturbation velocity need not vanish at the interface in the present case, and secondly, the tangential surface stresses need not be zero. The first modification should render the sub-layer less stable, since less restriction is placed on the disturbance, while the second modification should make the layer more stable, since a restoring stress can be exerted on the lower region by the fluid in the upper region. Clearly, the former effect predominates in the semi-infinite case. The actual value of the critical Rayleigh number for our sub-layer could be determined by calculating the growth rates for smaller and smaller Rayleigh numbers until the curve is reached whose maximum is tangent to the line $\sigma = 0$. However, a more general approach exists, as was discussed in an earlier section.

The wave numbers corresponding to the maximum growth rates are given in Table I.

P \ R	10^3	10^4	10^5
7.0	1.5	3.8	5.4
0.7	1.8	4.1	6.0

Table I. Wave Numbers of Fastest Growing Disturbances.

We observe that increasing the Rayleigh number increases the wave number of the fastest growing disturbance, while increasing the Prandtl number decreases this wave number.

Interpreting the Prandtl numbers of 0.7 and 7.0 as corresponding to air and water, respectively, we find that the ratio of the maximum growth rates is given by

$$\sigma_a/\sigma_w \approx 1/3 .$$

Then the absolute growth rates, $\sigma^* = \sigma(\varkappa/d^2)$, will be in the ratio

$$\frac{\sigma_a^*}{\sigma_w^*} = \frac{\sigma_a}{\sigma_w}\frac{\varkappa_a}{\varkappa_w} .$$

Since $\varkappa_a/\varkappa_w \approx 75$, we find that

$$\sigma_a^*/\sigma_w^* \approx 25 .$$

That is, disturbances will grow about 25 times faster in air than in water for a given temperature profile.

Finally, since we have observed that σ never exceeds σ_o, and since σ_o tends to zero at $a = R^{1/4}$, we conclude that a semi-infinite fluid will be stable to all infinitesimal disturbances for which

$$a \geq R^{1/4} . \qquad (65)$$

Thus, if a given disturbance has no Fourier components which violate the inequality (65), the disturbance will be damped out.

3. Velocity and Temperature Profiles

The velocity and temperature profiles have been obtained for the maximum growth-rate wave numbers given in Table I. In each case, the curves have been normalized so that the peak amplitude is unity.

Figure 11 shows the velocity curves for a Prandtl number of 7.0. At high Rayleigh numbers the penetration is quite small, but for the lower Rayleigh numbers the penetration depth is greatly increased. This result may be a consequence of the wave number assumed by the most prominent disturbance. The wave length of the disturbance is related to the wave number by the equation

$$\delta = 2\pi \frac{d}{a} \quad .$$

As we pointed out in the previous section, the wave numbers corresponding to the maximum growth rates are smallest for the low Rayleigh numbers. Thus, the wave lengths for these disturbances will be large.

The temperature profiles for P = 7.0 are shown in Figure 12. Although the same dependence on the Rayleigh number is exhibited, the temperature does not penetrate the stable layer as deeply as the velocity. The velocity and temperature perturbations are of the same sign, so that if we consider W as being positive, corresponding to the fluid rising against gravity, then the temperature is everywhere increased. In particular, at the heat source z = 0 the temperature gradient is rendered numerically smaller so that less heat will cross the surface z = 0 locally. In those regions of the fluid where the mo-

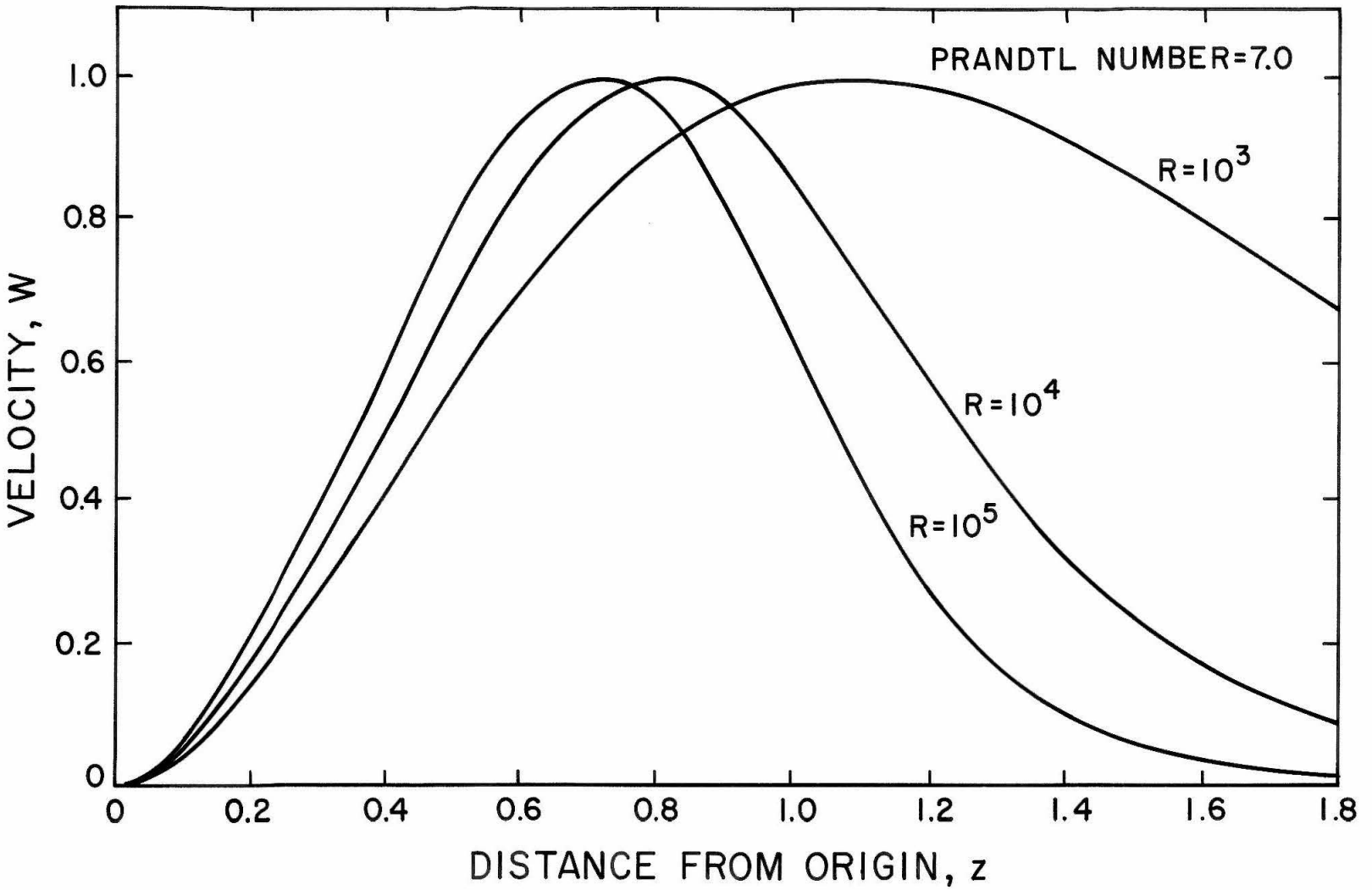

FIGURE II- VELOCITY PROFILE

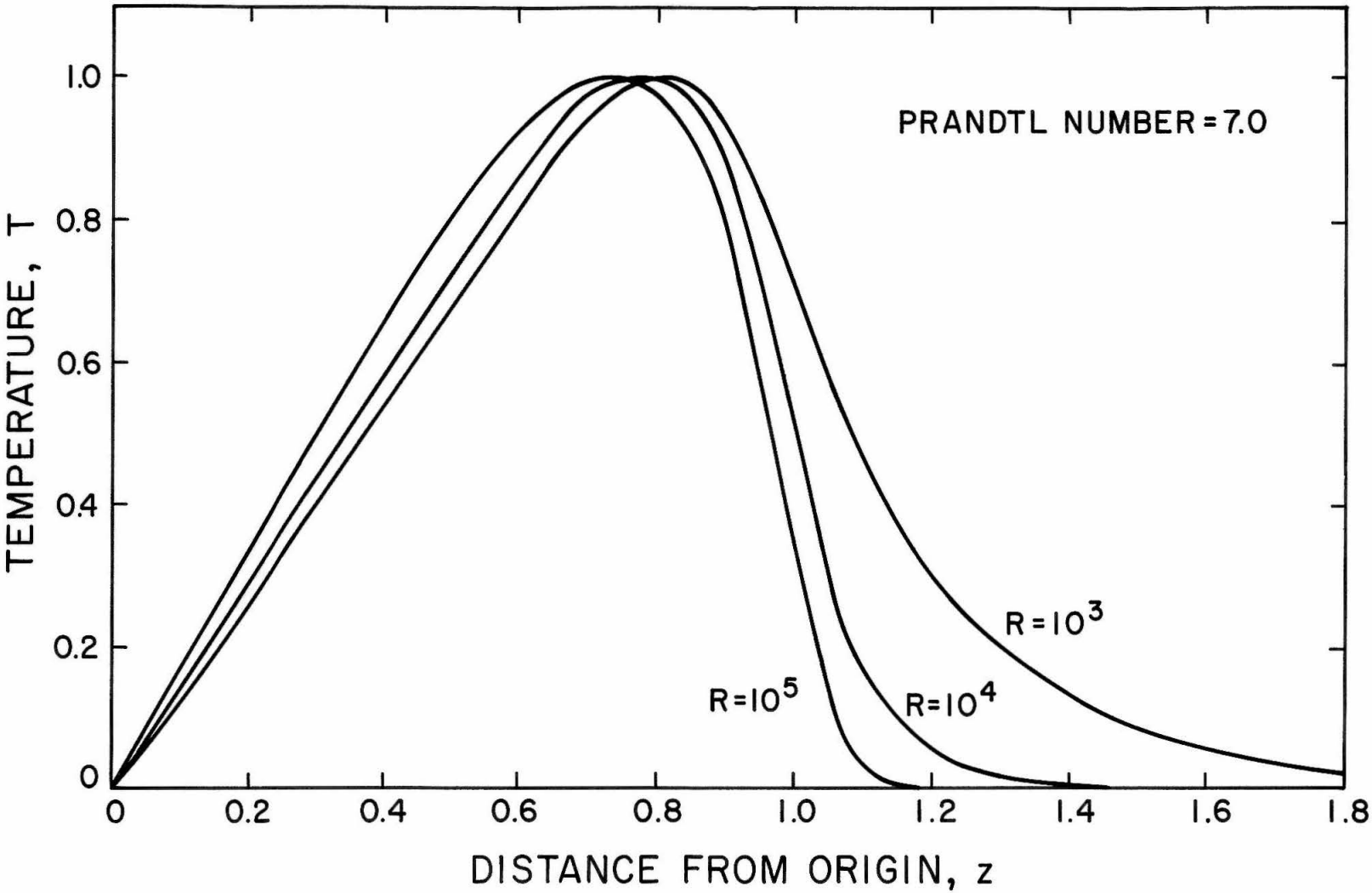

FIGURE 12 - TEMPERATURE PERTURBATION

tion is downward, the situation is reversed. Here, the temperature perturbation is negative, giving a decreased temperature profile and a greater local heat flux through the plane $z = 0$. Malkus and Veronis (1958) have shown that the finite amplitude effects are such that the net heat flux through the plane $z = 0$ is greater with convection than with conduction alone.

The results for the Prandtl number 0.7 are illustrated in Figures 13 and 14. Comparing these with Figures 11 and 12 shows that the lower Prandtl number shifts the entire velocity curve towards the origin so that the velocity does not penetrate so deeply. However, the temperature curve is flattened out so that the temperature is greater than that for $P = 7.0$, in both the region where dT/dz is positive and also where dT/dz is negative. In spite of this tendency for the velocity and the temperature penetrations to approach each other, there is still a much deeper velocity penetration than temperature penetration.

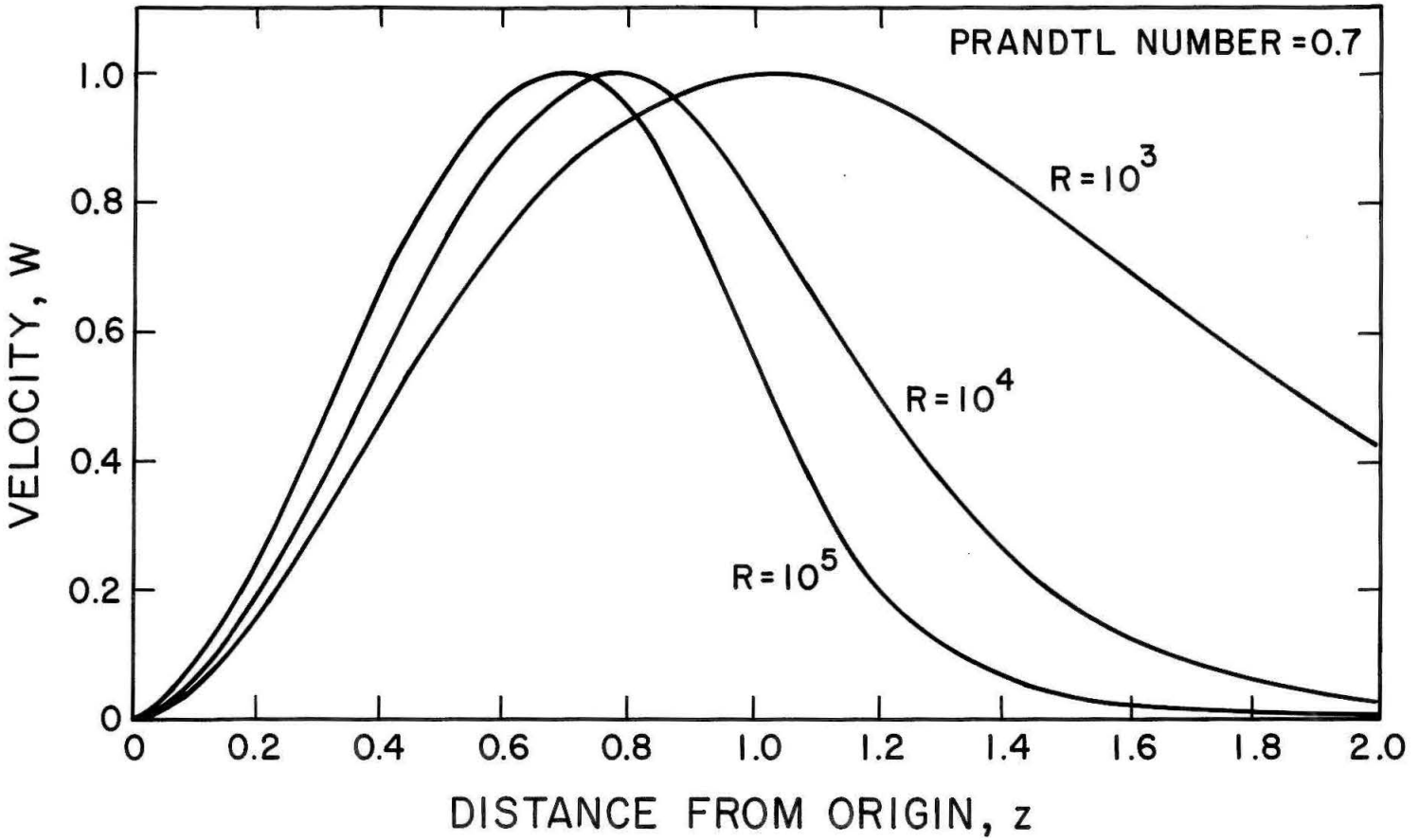

FIGURE 13 - VELOCITY PROFILE

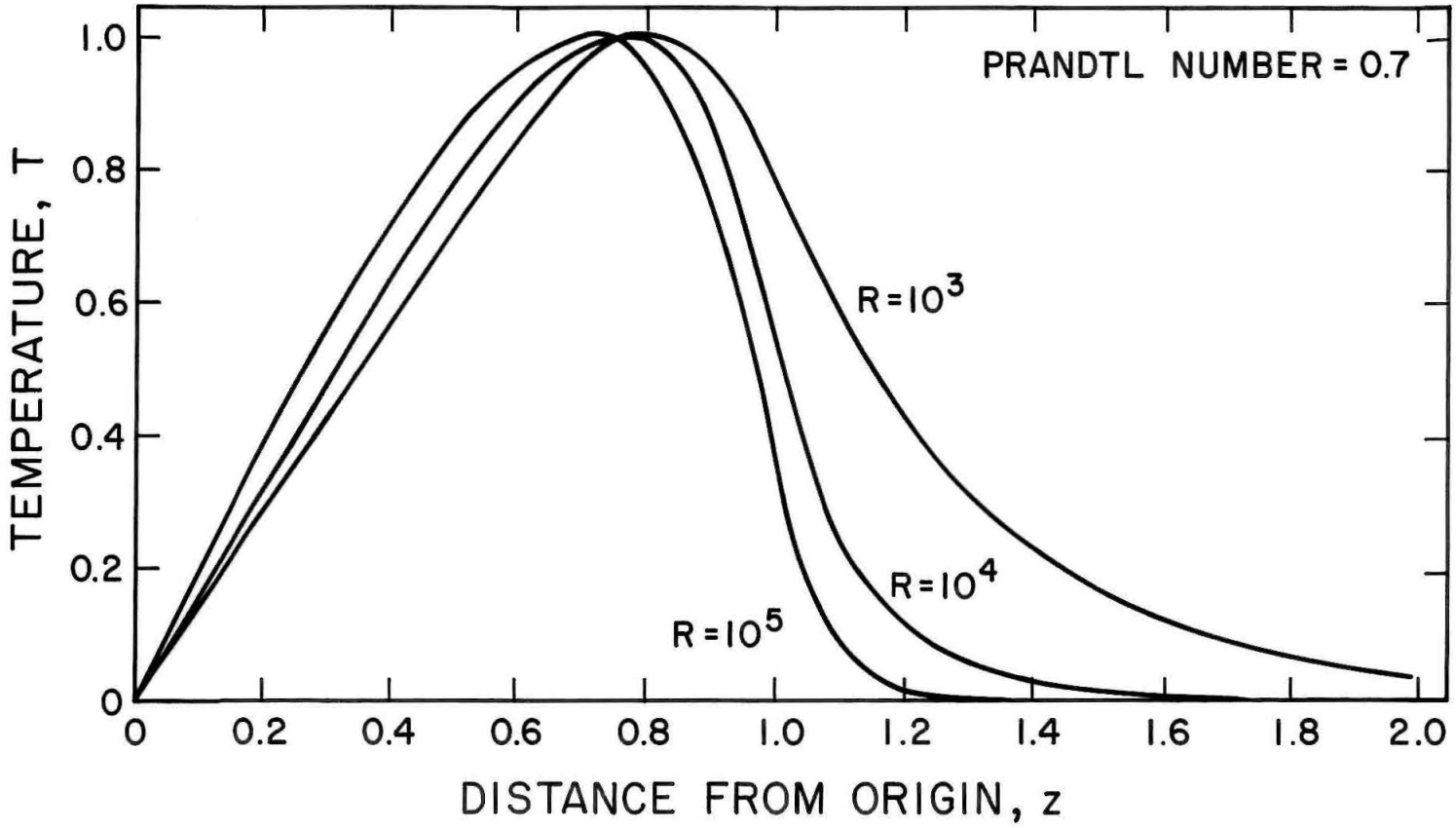

FIGURE 14 - TEMPERATURE PERTURBATION

4. Critical Rayleigh Number

There is only one root of the determinant (61) which is not a true eigenvalue, and this occurs when $R = a^4$. Inspection of equation (55) shows that when this occurs, γ_1 will be zero, so that two columns of the determinant (61) will be identical. Roots of (61) corresponding to σ_1 cannot exist here, since γ_2 and γ_3 are complex conjugates for all values of R and a, so they can never coalesce.

For a given wave number, an infinite set of discrete values of R exist which reduce the determinant (61) to zero. These correspond to different modes of instability and are the counterpart of the infinite set of growth rates encountered previously. By the definition of the critical Rayleigh number, we are interested in the numerically smallest value out of this discrete set. This gives the lowest mode of instability, which corresponds to the largest growth rates obtained earlier.

For the lowest mode of instability, there is a continuous spectrum of Rayleigh numbers which render the determinant (61) equal to zero, one for each wave number. These solutions correspond to the points where the positive growth-rate curves cross the line $\sigma = 0$. For a fixed value of R, this will occur at two different wave numbers. As we pointed out earlier, it is the minimum value of R with respect to the wave number a that gives the critical Rayleigh number.

A typical solution curve, for fixed ζ, is shown in Figure 15. We denote the critical value of R by R_c and the corresponding critical wave number by a_c.

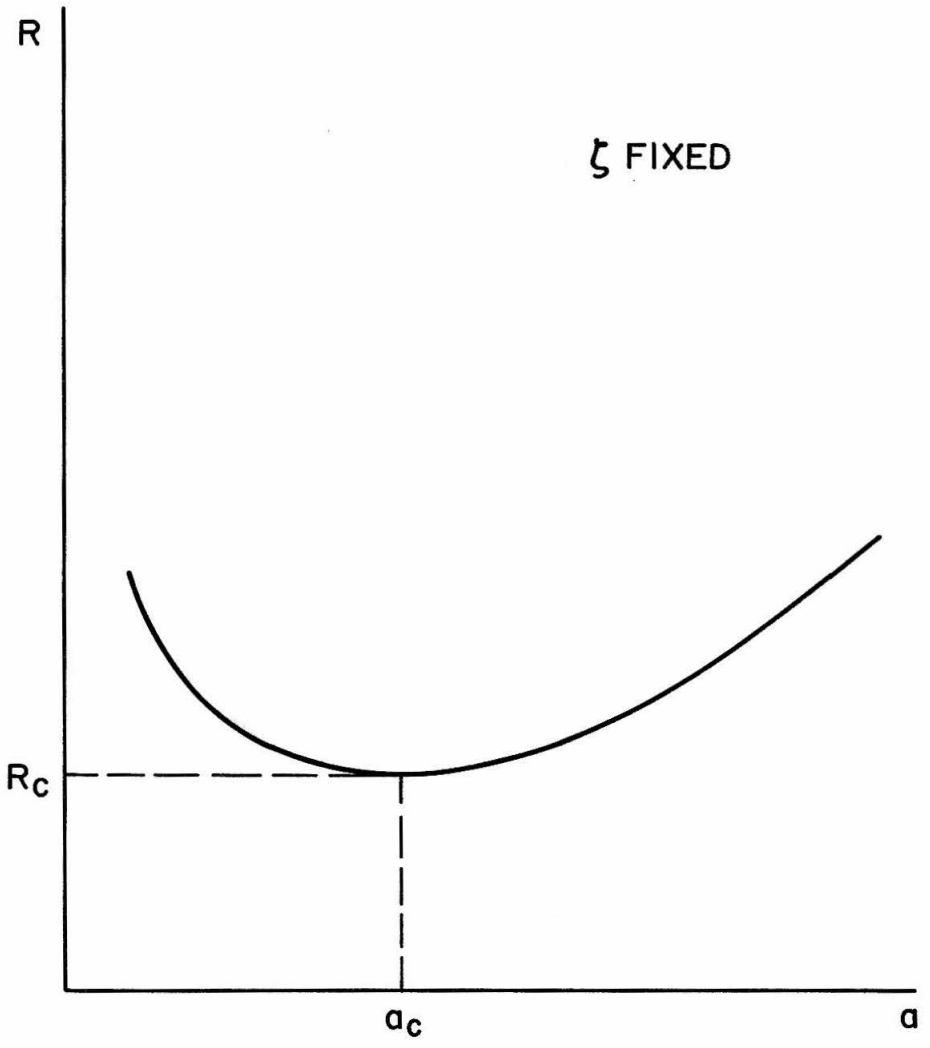

FIGURE 15-DETERMINATION OF CRITICAL RAYLEIGH NUMBER

The variation of critical Rayleigh number with ζ is shown in Figure 16, and the corresponding wave numbers are presented in Figure 17. The critical Rayleigh number decreases monotonically from a value of 1707.8 at $\zeta = 1$ to a value of 32 at $\zeta = \infty$. The latter limit corresponds to the semi-infinite fluid. The wave number corresponding to the critical Rayleigh number decreases almost linearly from a value of 3.117 at $\zeta = 1$ to zero at $\zeta = \infty$.

For discussion of marginal stability of a finite fluid layer, it is convenient to base the Rayleigh number and the wave number on the length scale h, the depth of the fluid layer. Thus, we introduce new parameters defined by

$$\tilde{R} = \frac{h^3}{d^3} R = \frac{\alpha g (T_o^* - T_1^*) h^3}{\kappa \nu}$$

$$\tilde{a} = \frac{h}{d} a = \frac{2\pi\delta}{h}$$

$$\epsilon = \frac{1}{\zeta} = \frac{d}{h}$$

Transforming the results of Figures 16 and 17 to the new parameters $\tilde{R}$, $\tilde{a}$, and ϵ gives the results shown in Figures 19 and 20. If we had used the length scale h instead of d, equations (51), (52), (58), (59), and (60) would have read

$$(D^2 - \tilde{a}^2)^3 W_1 = -\tilde{a}^2 \tilde{R} W_1$$

$$(D^2 - \tilde{a}^2)^3 W_2 = 0 \ .$$

On $z = 0$;

$$W_1 = DW_1 = D^2(D^2 - 2\tilde{a}^2)W_1 = 0$$

on $z = \epsilon$;

$$(W_1 - W_2) = (D^n W_1 - D^n W_2) = 0 \qquad n = 1, 2, 3, 4, 5$$

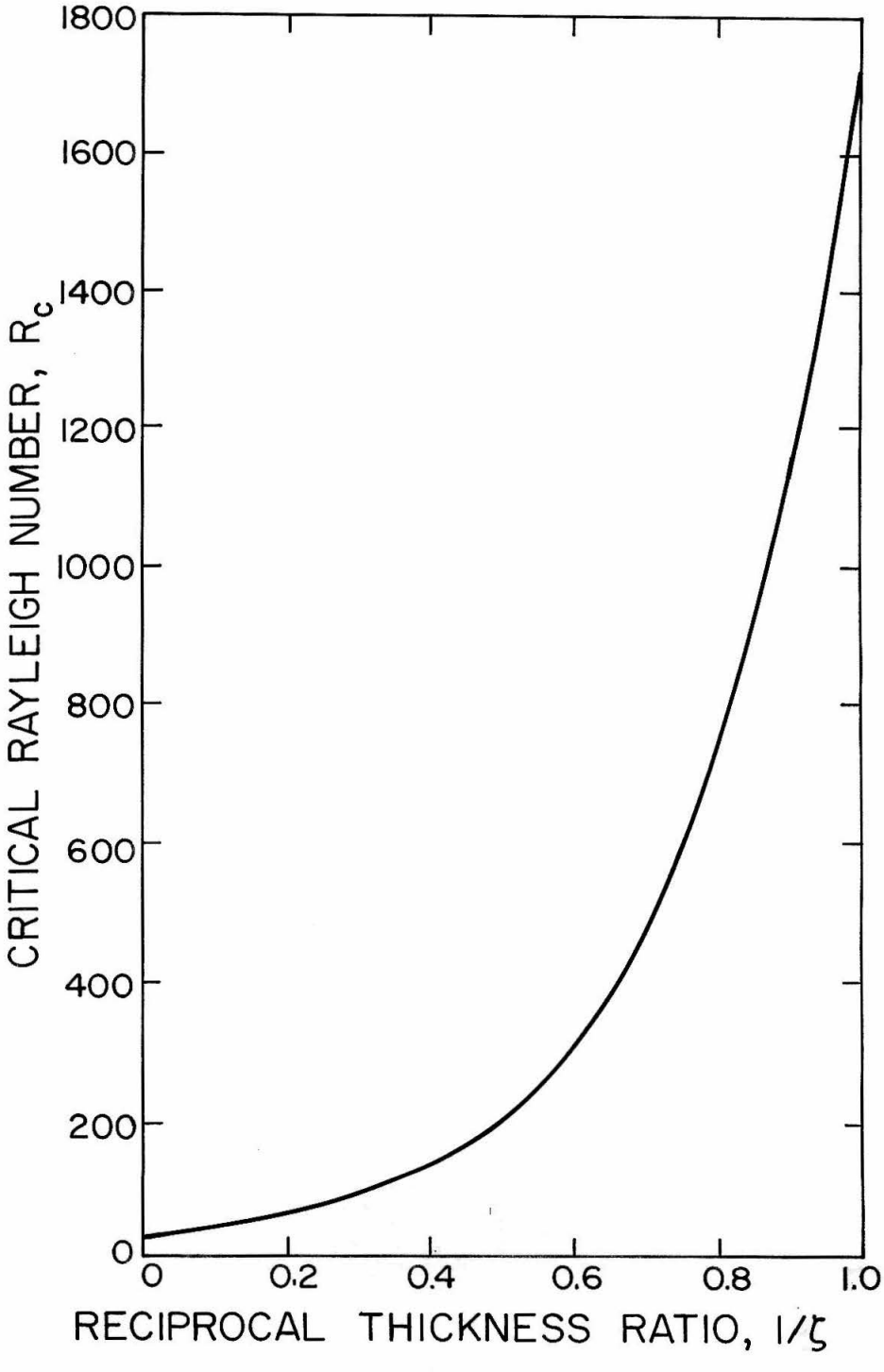

FIGURE 16 - CRITICAL RAYLEIGH NUMBER

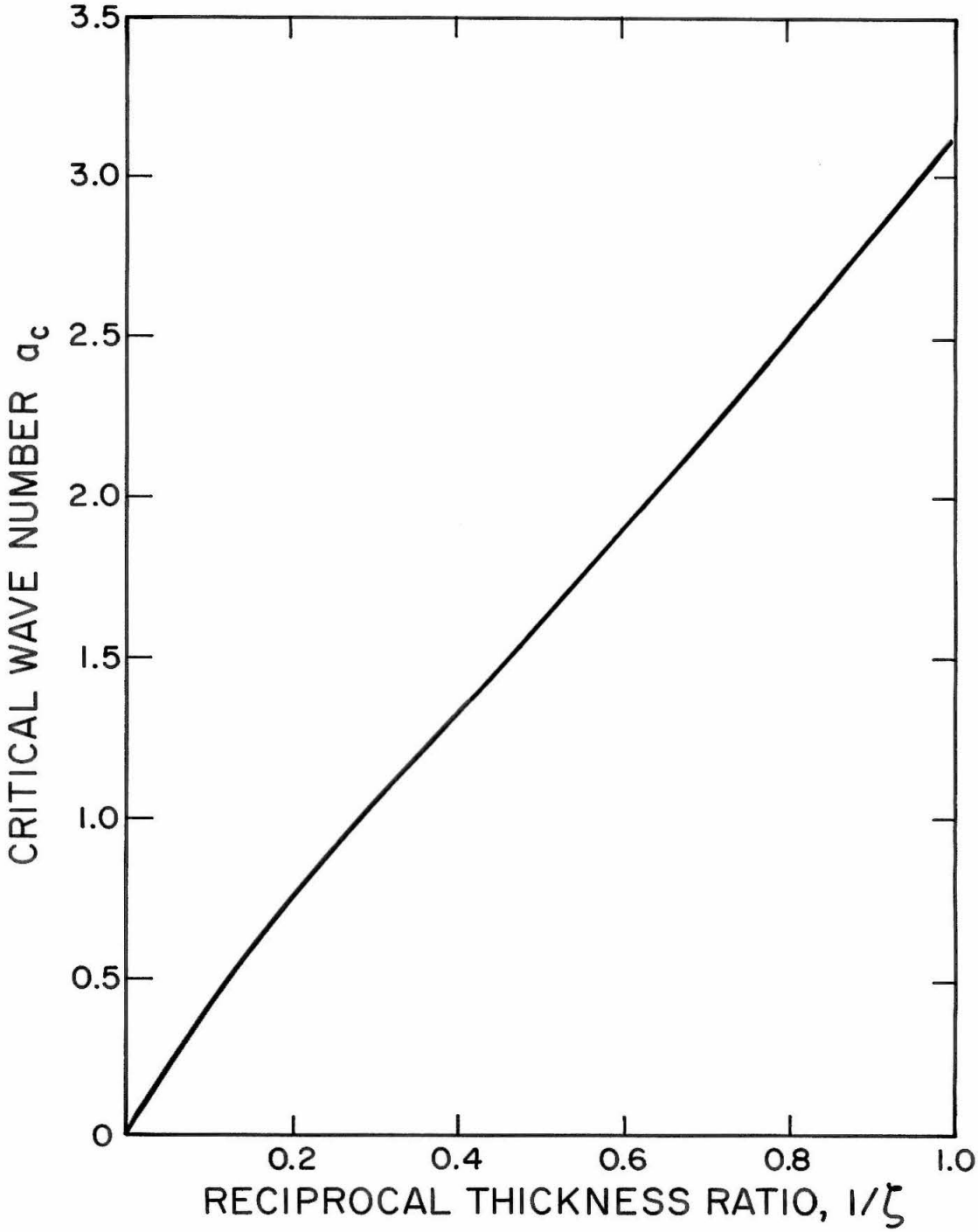

FIGURE 17 - CRITICAL WAVE NUMBER

on $z = 1$;

$$W_2 = DW_2 = D^2(D^2 - 2\tilde{a}^2)W_2 = 0$$

where now W_1, W_2 and z are non-dimensionalized by using h instead of d. From the above equations, we see that the results shown in Figures 16 and 17 apply to the situation depicted in Figure 18(a), where the plane $z = \zeta$ is considered movable, while the results of Figures 19 and 20 apply directly to the situation shown in Figure 18(b), where the plane $z = \epsilon$ is considered movable. The latter case corresponds to a moving conduction temperature profile between fixed boundaries.

Although the results of Figures 16 to 20 could theoretically be obtained by use of either length scale, it was found that numerical difficulties arose in case (b) when ϵ became small. These difficulties are related to the numerically large values of R_c shown in Figure 19, for small ϵ, and lead to an indeterminate value of R_c for the semi-infinite case. These difficulties did not arise in case (a).

In Figure 19, the minimum critical Rayleigh number is 1340 and occurs at $\epsilon = 0.72$. For a given method of heating, the corresponding solution to the heat conduction equation will trace a path on Figure 19 which, for an initially isothermal fluid, will emanate from the origin. The intersection of this heat conduction curve with the critical Rayleigh number curve will determine the actual critical Rayleigh number. However, for the present, we may state that, for infinitesimal disturbances,

$$\tilde{R}_c \geq 1340 \ . \qquad (66)$$

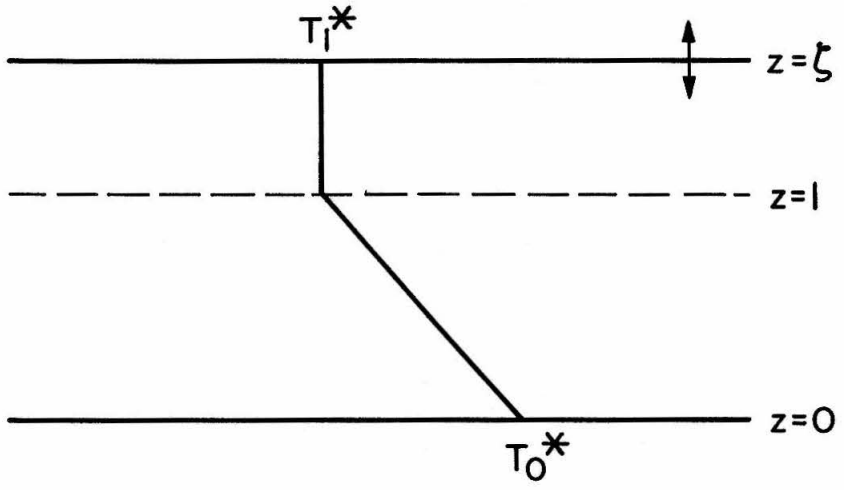

(a) $z=\zeta$ MOVABLE

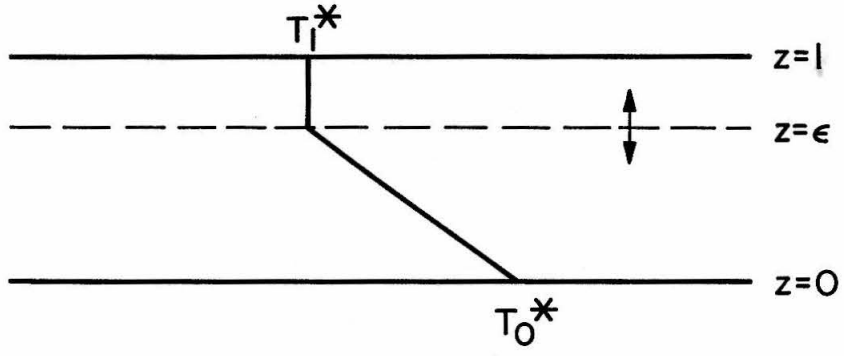

(b) $z=\epsilon$ MOVABLE

FIGURE 18-NATURE OF BOUNDARIES FOR FINITE FLUID LAYER

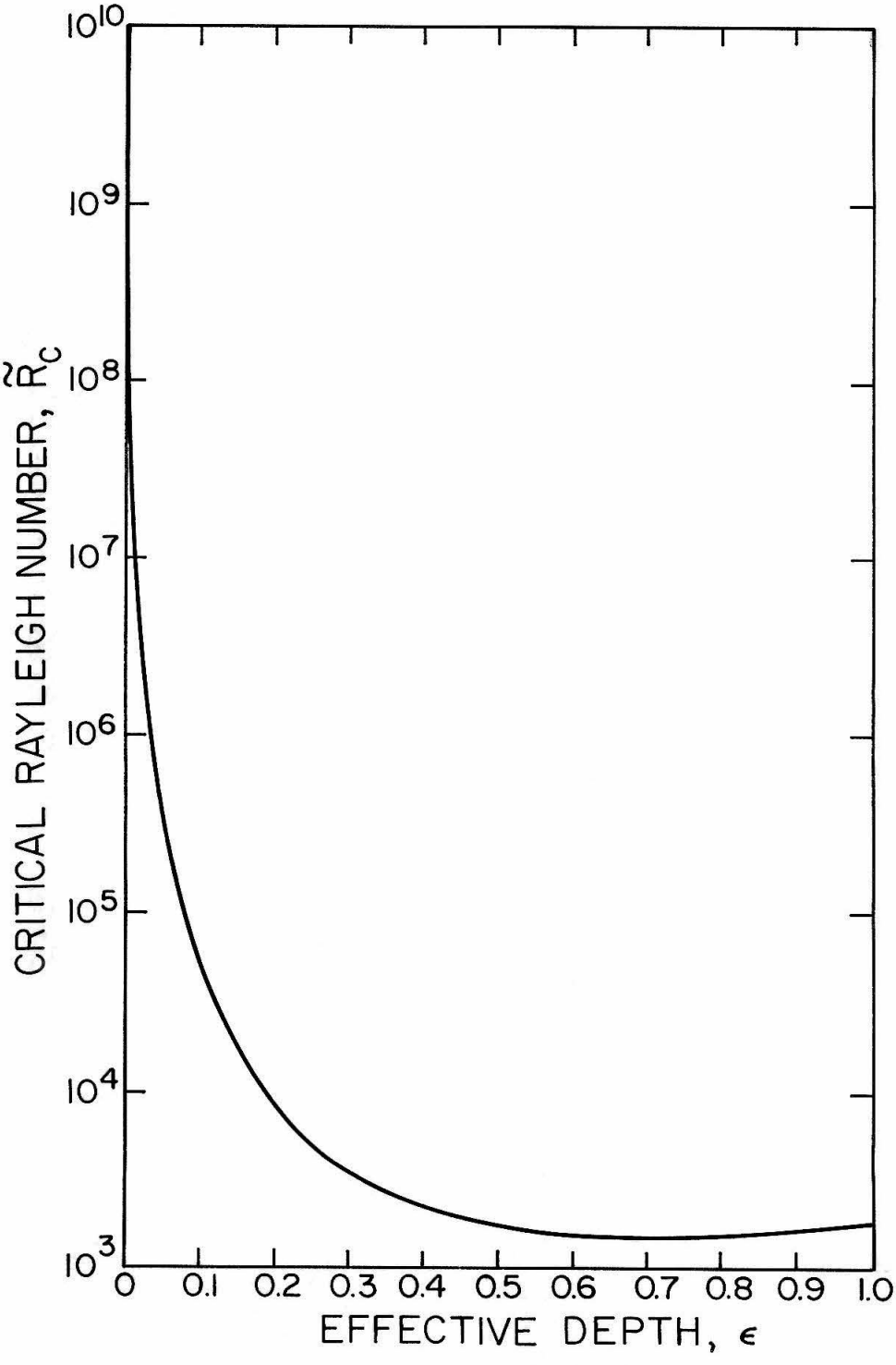

FIGURE 19 - CRITICAL RAYLEIGH NUMBER

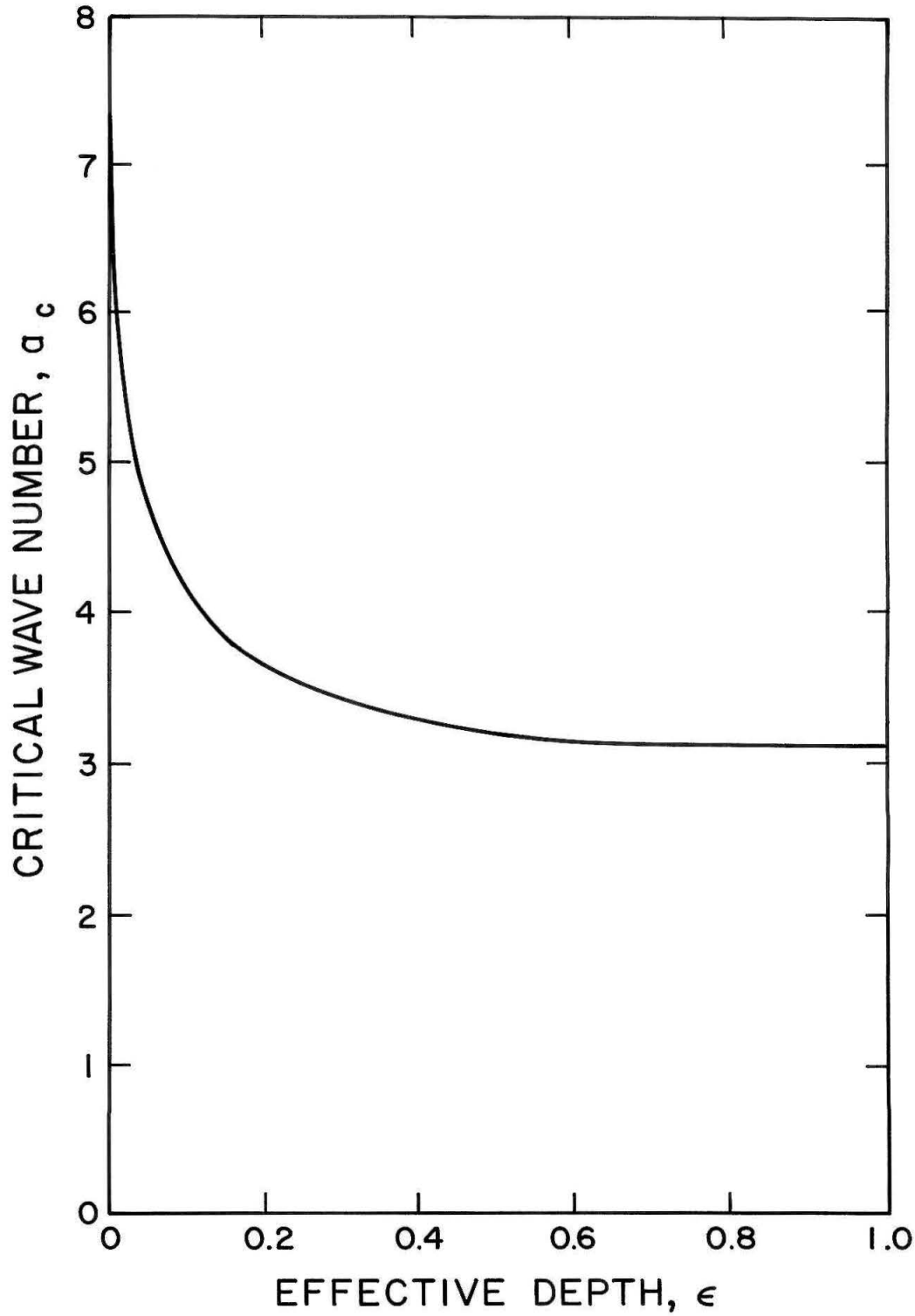

FIGURE 20 - CRITICAL WAVE NUMBER

IV. COMPARISON WITH EXPERIMENTS

1. Review of Experimental Results

In order that we may compare the results of the previous sections with the relevant experimental results, a more detailed description of the previously mentioned anomalies will be presented here, including the numerical data.

Although Graham (1933) appears to have been the first to note the existence of a non-cellular mode of thermal convection, the first relevant data were published by Chandra (1938). The experiments performed by Chandra involved a layer of air bounded above by a glass plate and below by a steel plate. Below the lower surface there were a number of heating coils enclosed in an asbestos box. Side walls were erected from the upper surface so that water could be kept in contact with the glass. In this way, the bounding surfaces could be maintained at uniform, but different, temperatures while the motion of the fluid could be observed from above with the aid of injected smoke. The temperatures were measured at midpoint and as close to the top and bottom plates as possible by means of platinum resistance thermometers.

The temperature differences measured by Chandra, which correspond to sustained convection, are shown in Figure 21 along with the linear temperature profile theory. The relation of these data to those for the onset of instability is unknown, since Chandra's experimental procedure is made clear by the following quotation from his publication. "In practice it was found easier to estimate the limiting value by first heating the bottom plate until the difference of

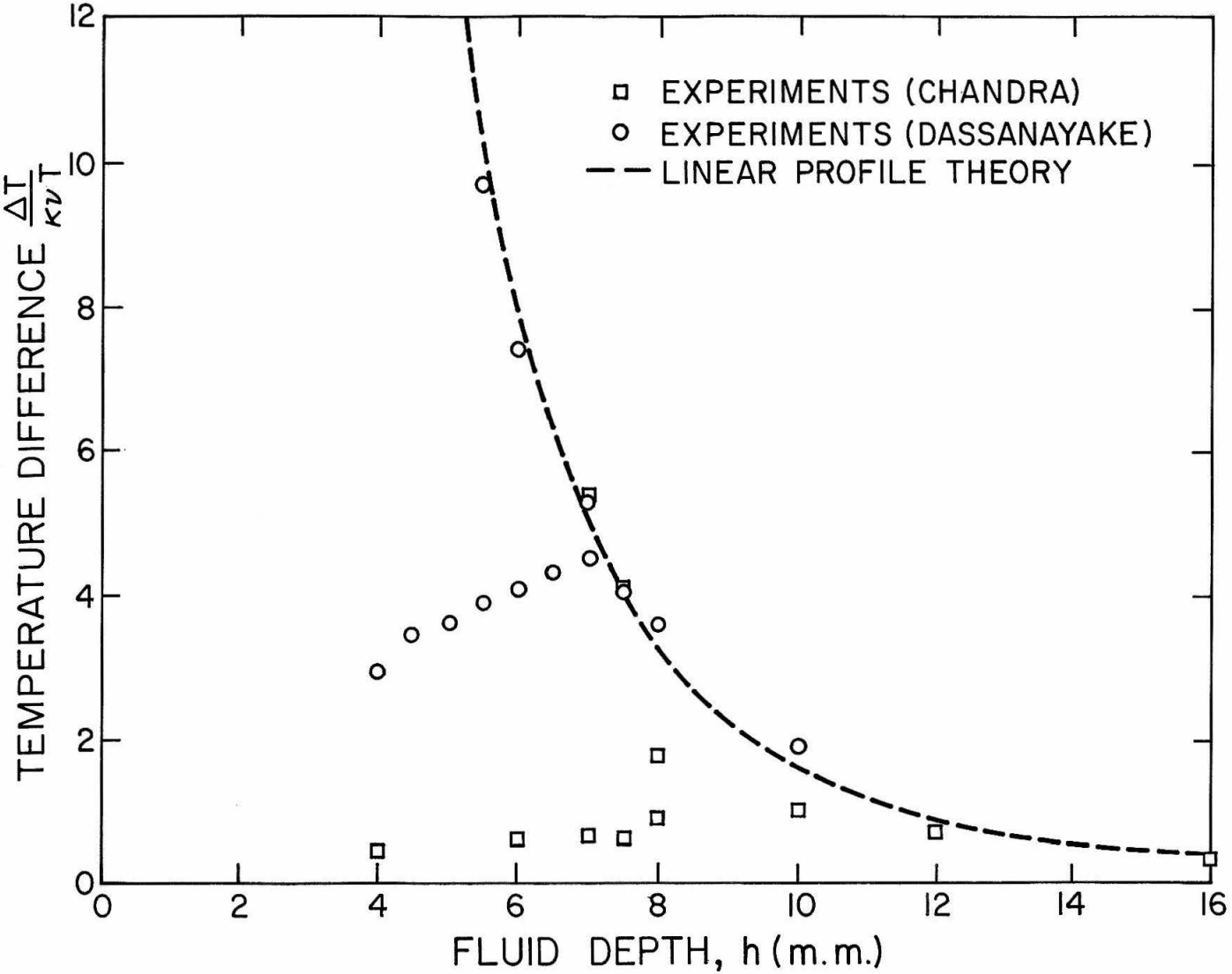

FIGURE 21 - DATA FOR MAINTAINED COLUMNAR CONVECTION

temperature was sufficient to produce motion, then allowing the metal plate to cool slowly. The critical stage at which all motion had just ceased could then be observed, and the corresponding difference of temperature measured."

For $h \leq 6$ mm, Chandra observed that a columnar mode of instability was induced and was sustained at temperature differences considerably less than predicted by the classical analysis. Increasing the temperature difference in this range resulted only in increased activity of the columnar mode. For $h \geq 10$ mm, the instability was of the cellular mode and corresponded closely to the classical predictions. For $6\,\text{mm} < h < 10\,\text{mm}$, the columnar mode could be established at temperature differences lower than predicted by the theory, while increasing the temperature difference resulted in a transition to the cellular mode at temperatures close to the theoretical values.

Using essentially the same apparatus as Chandra, Dassanayake performed similar tests using carbon dioxide rather than air. The same qualitative behavior was observed.

The experiments of de Graaf and van der Held (1953) were concerned with the rate of heat transfer across plane air layers. However, in the course of these experiments, it was noted that a columnar motion could be induced at layer thicknesses of 5.5 and 6.9 mm if the Rayleigh number exceeded 1400. This result has already been explained by the present analysis without further calculation. It was observed that the minimum of the curve of Figure 19 resulted in the inequality (66), namely,

$$\tilde{R}_c \geq 1340 \ .$$

This is in close agreement with the observations of de Graaf and van der Held.

Soberman (1959) measured the critical Rayleigh number for various rates of heating. Two fluids were used, silicon oil and mercury. The fluid was placed in a cylindrical container which had heating elements below its bottom surface. The upper surface of the fluid was open to the atmosphere, and it was noted that a surface scum formed during the tests. Two fluid depths were considered, 1/2 inch and 1 inch. Temperatures were measured by means of two thermopiles which were located in the fluid at 1/8 inch and 3/8 inch from the fluid surfaces for fluid depths of 1/2 inch and 1 inch respectively. The computed Rayleigh numbers were based on a linear temperature variation across the fluid layer. Heat was applied by suddenly admitting power to the heating coils, which had a small air gap between them and the bottom of the container to achieve uniform heating. Soberman correlated his results with the equation

$$\tilde{R}_c = 90.7 \left(\frac{\alpha g Q h^4}{2\kappa\nu k}\right)^{0.394} .$$

The actual experimental points are recorded in Figure 22 for future comparison.

The experiments of Spangenberg and Rowland (1961) were carried out with a 10 cm layer of water. The water was contained in a rigid vessel and a cover could be placed over the surface of the water. Under initially isothermal conditions, the cover was suddenly removed. The subsequent surface evaporation caused a transient cooling of the upper surface. The surface temperature of the water

was measured using a schlieren system, while two thermopile assemblies measured the temperatures within the fluid. The initial motion of the fluid was observed to be mainly in the form of two-dimensional sheets of plunging fluid emanating from the free surface, but a few three-dimensional columns, of the type observed by Chandra, were also observed. Since the rate of cooling was not controlled, only one set of data could be recorded for the onset of instability. This data showed that the surface temperature decreased approximately linearly in time, reaching a depression of 0.36°C after 70 seconds, at which time the instability was first observed. At this point, the effective depth of the temperature profile was about 5 mm. The stability point arising from the foregoing data is plotted in Figure 23(b) for future discussion.

When the apparatus was left undisturbed for several hours, the motion was observed to reach a quasi-steady form. Sheets of cold liquid were observed to plunge at regular intervals, the leading edge of each plume descending as far as the bottom of the container, where it broke up into intertwining filaments and then dissipated. At this stage, the temperature depression of the upper surface was only 0.1°C and the effective depth about 2 mm. The quasi-steady motion persisted even when the apparatus was left undisturbed for several days.

2. Constant Flux Heating

The results of Soberman (1959) seem to correspond approximately to the idealized case of constant heating. Then the conduction phase will be described by the solution of the following problem.

$$\frac{\partial T^{*(o)}}{\partial t^*} = \varkappa \frac{\partial^2 T^{*(o)}}{\partial z^{*2}}$$

$$\left.\begin{aligned} -k \frac{\partial T^{*(o)}}{\partial z^*}(0, t^*) &= Q \\ T^{*(o)}(h, t^*) &= T_1^* \end{aligned}\right\} \quad t^* > 0$$

$$T^{*(o)}(z^*, 0) = T_1^* \qquad 0 \le z^* \le h$$

The solution to this problem is

$$T^{*(o)}(z^*, t^*) = T_1^* + \frac{Qh}{k}\left(1 - \frac{z^*}{h}\right) - \frac{Qh}{k} \sum_{n=0}^{\infty} \frac{8}{(2n+1)^2 \pi^2} e^{-(2n+1)^2 \frac{\pi^2 \varkappa}{4h^2} t^*} \cos (2n+1) \frac{\pi z^*}{2h} .$$

Introduce dimensionless variables defined by $t^* = \frac{h^2}{\varkappa} t$, $z^* = hz$, $T^{*(o)} = \frac{Qh}{k} T^{(o)}$. In terms of these variables the solution to the heat conduction equation becomes

$$T^{(o)}(z, t) = T_1 + (1-z) - \sum_{n=0}^{\infty} \frac{8}{(2n+1)^2 \pi^2} e^{-(2n+1)^2 \frac{\pi^2}{4} t} \cos (2n+1) \frac{\pi}{2} z . \tag{67}$$

The definition of the Rayleigh number is

$$\tilde{R}(t) = \frac{\alpha g Q h^4}{\varkappa \nu k} \left\{ T^{*(o)}(0, t^*) - T_1^* \right\} .$$

From this definition and equation (67) we have

$$\tilde{R}(t) = \frac{\alpha g Q h^4}{\varkappa \nu k} \left\{ 1 - \sum_{n=0}^{\infty} \frac{8}{(2n+1)^2 \pi^2} e^{-(2n+1)^2 \frac{\pi^2}{4} t} \right\} . \tag{68}$$

From the definition of the effective depth ε we have

$$\varepsilon(t^*) = \frac{\int_0^h T^{*(o)}(z^*, t^*) dz^*}{h\{T^{*(o)}(0, t^*) - T_1^*\}} .$$

Thus, using equation (67), we find

$$\varepsilon(t) = \frac{1 - \sum_{n=0}^{\infty} \frac{(-1)^n 32}{(2n+1)^3 \pi^3} e^{-(2n+1)^2 \frac{\pi^2}{4} t}}{1 - \sum_{n=0}^{\infty} \frac{8}{(2n+1)^2 \pi^2} e^{-(2n+1)^2 (\pi^2/4) t}} . \tag{69}$$

For a given value of t, $\tilde{R}$ may be calculated from equation (68) and ε may be calculated from equation (69). Then, as t varies from zero to infinity, the heat conduction equation traces a monotonically increasing curve on Figure 19 which varies from $\tilde{R} = \varepsilon = 0$ at $t = 0$ to $\tilde{R} = (\alpha g Q h^4)/(\varkappa \nu k)$, $\varepsilon = 1.0$ at $t = \infty$. The point at which this curve intersects the critical Rayleigh number curve gives the theoretical value of $\tilde{R}_c$ and the corresponding critical time, t_c. The location of this point will depend on the magnitude of the parameter $(\alpha g Q h^4)/(\varkappa \nu k)$, and a value of $\tilde{R}_c$ will exist for each value of this parameter. The resulting stability curve so obtained is shown in Figure 22 for critical times varying from about 4×10^{-4} to infinity. The experimental results of Soberman are also shown in this figure.

There is one major feature about Soberman's results which accounts for, at least in part, the discrepancy between the theoretical

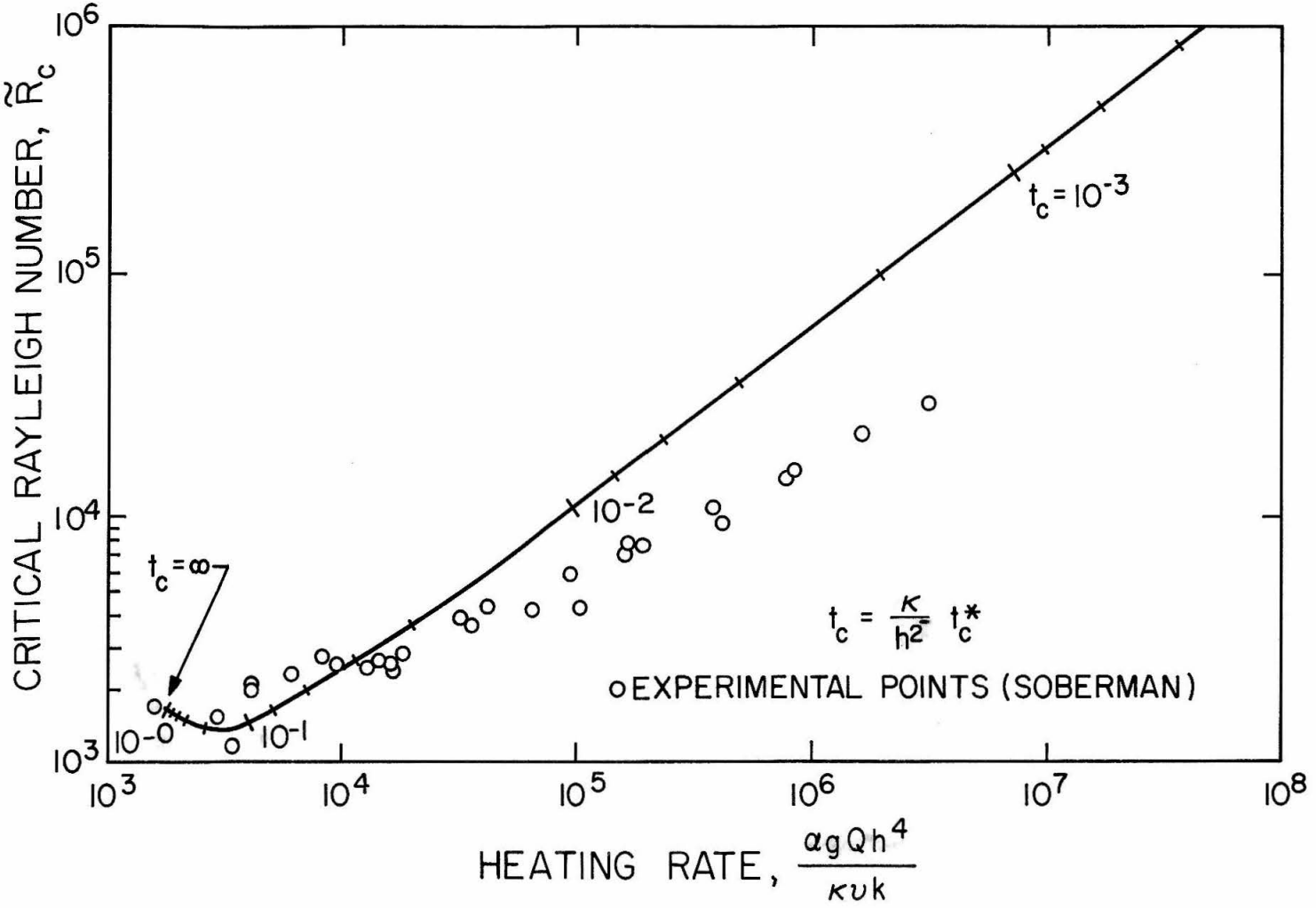

FIGURE 22 - STABILITY CURVE FOR CONSTANT FLUX HEATING

and experimental results. This feature involves the way in which the values of $\tilde{R}_c$ were calculated from the experimental data. Soberman assumed that the temperature profile at criticality was approximately linear for all rates of heating, so that the overall temperature difference was estimated by linearly extrapolating the temperature difference between the thermopiles. As was mentioned earlier, the thermopiles were located 1/8 inch and 3/8 inch from the fluid surfaces when the fluid depth was 1/2 inch and 1 inch, respectively. Thus, any curvature in the temperature profile would result in an underestimated value of the Rayleigh number. This effect will be particularly important for large values of the heating parameter, which corresponds to short manifestation times, since the non-linearity of the temperature profile is then more pronounced. Thus, near the upper portion of the curve in Figure 22, we would expect the experimental values of $\tilde{R}_c$ to be smaller than the theoretical values, which is indeed the case.

In view of the foregoing discussion, it may be concluded that the theoretical and experimental results are in agreement and that for constant flux heating, rapid rates of heating result in high critical Rayleigh numbers.

3. Uniformly Increasing Surface Temperature

The results of Spangenberg and Rowland (1961) show that the temperature of the upper surface decreased approximately linearly with time up to the onset of convection. Thus, treating the analogous case of heating from below, the conduction temperature will be given by the solution of the following problem.

$$\frac{\partial T^{*(o)}}{\partial t^*} = \kappa \frac{\partial^2 T^{*(o)}}{\partial z^{*2}}$$

$$\left.\begin{aligned} T^{*(o)}(0, t^*) &= T_1^* + \beta_1 t^* \\ T^{*(o)}(h, t^*) &= T_1^* \end{aligned}\right\} \quad t^* > 0$$

$$T^{*(o)}(z^*, 0) = T_1^* \qquad 0 \le z^* \le h$$

The solution to this problem is

$$T^{*(o)}(z^*, t^*) = T_1^* + \left(1 - \frac{z^*}{h}\right)\beta_1 t^* - \beta_1 \frac{h^2}{\kappa} \sum_{n=1}^{\infty} \frac{2}{n^3 \pi^3} \sin \frac{n\pi z^*}{h} \left(1 - e^{-\frac{n^2 \pi^2 \kappa}{h^2} t^*}\right)$$

Introduce dimensionless variables defined by $t^* = \frac{h^2}{\kappa} t$, $z^* = hz$, $T^{*(o)} = [(\beta_1 h^2)/\kappa] T^{(o)}$. In terms of these new variables the above equation becomes

$$T^{(o)}(z, t) = T_1 + (1-z)t - \sum_{n=1}^{\infty} \frac{2}{n^3 \pi^3} \sin n\pi z \left(1 - e^{-n^2 \pi^2 t}\right) . \tag{70}$$

From equation (70) and the definitions of the Rayleigh number $\tilde{R}$ and the effective depth ε, we find

$$\tilde{R}(t) = \frac{\alpha g \beta_1 h^5}{\kappa^2 \nu} t \tag{71}$$

$$\epsilon(t) = 1 - \frac{8}{t} \sum_{n=0}^{\infty} \frac{1}{(2n+1)^4 \pi^4} \{1 - e^{-(2n+1)^2 \pi^2 t}\} \qquad (72)$$

For a given value of t , $\tilde{R}$ and ϵ may be calculated from equations (71) and (72), respectively. Then, as t varies from zero to infinity, the solution (70) traces a monotonically increasing curve on Figure 19 which varies from $\tilde{R} = \epsilon = 0$ at $t = 0$ to $\tilde{R} = \infty$, $\epsilon = 1.0$ at $t = \infty$. Thus, there will be one location for each value of the parameter $(\alpha g \beta_1 h^5)/(\kappa^2 \nu)$ where the heat conduction curve intersects the marginal stability curve. The trace of these points is shown in Figures 23a and 23b for critical times varying from about 10^{-4} to 10^{+1}. The experimental point arising from the results of Spangenberg and Rowland is also shown in Figure 23b.

The analytical results show that for values of $(\alpha g \beta_1 h^5)/(\kappa^2 \nu)$ less than 10^3, that is, for critical times greater than about unity, the critical Rayleigh number is independent of the heating rate. This is as we would expect, since for slow heating the temperature profile will remain essentially linear at all times. For values of the heating parameter lying between about 10^3 and 10^4, the critical Rayleigh number is slightly reduced. For large heating rates, greater than about 10^4, the critical Rayleigh number may be considerably increased over the classical value.

The numerical values of the critical Rayleigh number and the associated critical time are shown in Table II for the value of the heating parameter relevant to the experiments of Spangenberg and Rowland.

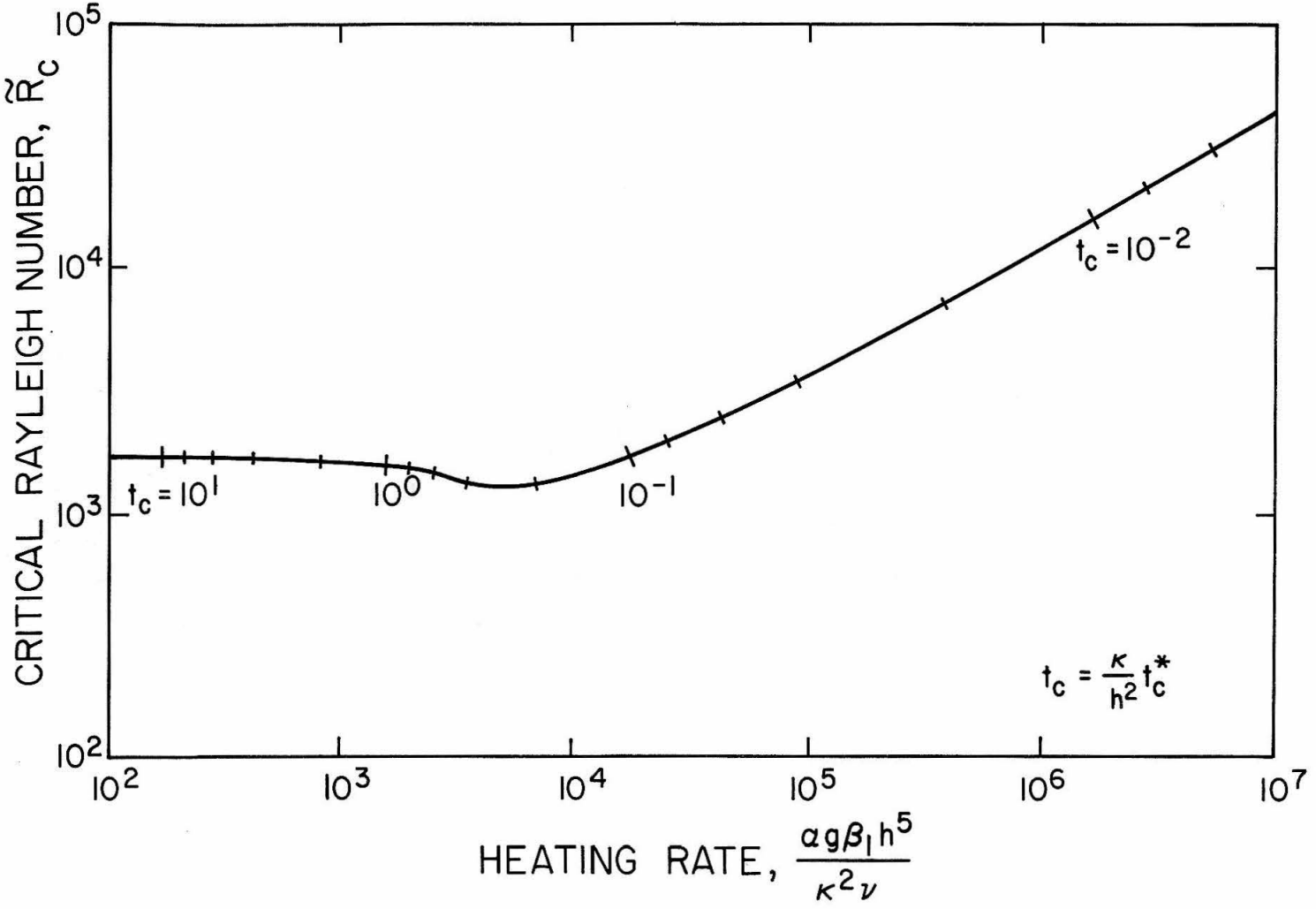

FIGURE 23a – STABILITY CURVE FOR UNIFORMLY INCREASING TEMPERATURE

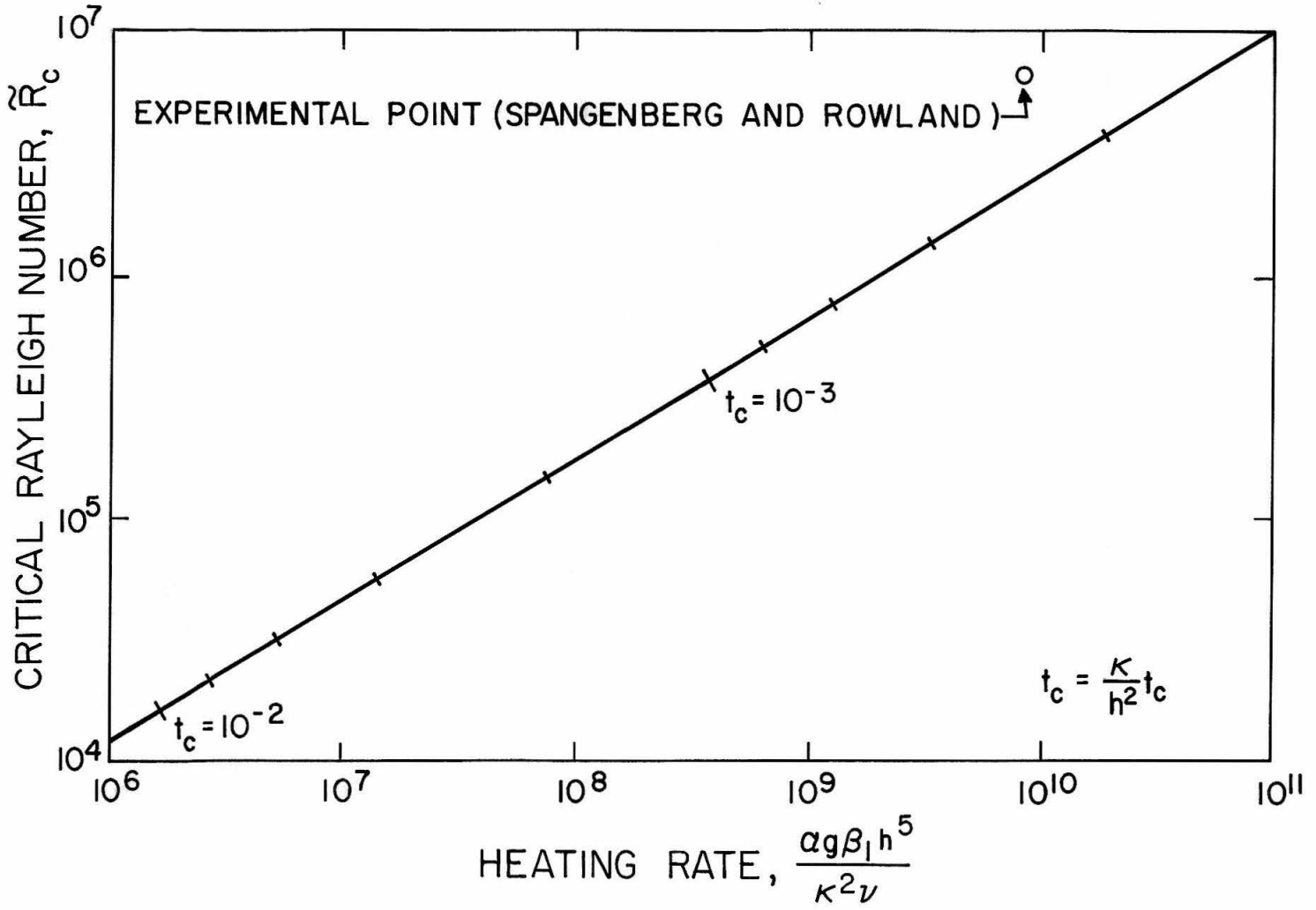

FIGURE 23b – STABILITY CURVE FOR UNIFORMLY INCREASING TEMPERATURE

	Experiment	Present Theory	Classical Theory
$\tilde{R}_c$	6.47×10^6	2.3×10^6	1.71×10^3
t_c^* (secs)	70	20	0.0157

Table II. Data for Onset of Instability in Evaporating Water.

The analysis based on the non-linear temperature profile theory gives results of the same order of magnitude as the experimental results. Furthermore, the remaining discrepancy can be accounted for qualitatively. The theory predicts the Rayleigh number and time at which infinitesimal disturbances will no longer be damped out, but which will allow one Fourier component to survive undamped. On the other hand, in order to observe visually a convective motion, this infinitesimal disturbance must have subsequently grown by two or three orders of magnitude. Now during the time required for this growth, the temperature of the lower surface, and hence the Rayleigh number, continues to increase uniformly. Thus the observation of a higher Rayleigh number and a larger critical time than predicted by the theory is self-consistent and understandable.

4. Maintained Non-Cellular Convection

So far, we have succeeded in giving an analytical explanation for all of the previously mentioned anomalies, except for the results of Chandra and Dassanayake, Figure 21. The successful analysis has been based on the theory that, due to the heating process, a non-linear temperature profile may exist in the fluid at the time instability first sets in. This being the case, we would not expect the initial mode of motion assumed by the fluid to correspond to the steady state mode of motion, since the temperature profile will continue to change due to continued conduction as well as the onset of convection. In cellular convection, on the other hand, the conduction temperature profile is approximately linear and steady, so that there is no tendency for the average temperature profile to change after convection is initiated.

Thus, on theoretical grounds alone, we would not expect the results of Figure 21 to correspond to the data prevailing at the onset of convection. This expectation is substantiated by the observations of Spangenberg and Rowland that the steady-state temperature difference may be considerably less than the value existing at the onset of convection. Moreover, it was observed that the sustained temperature gradient was highly non-linear, varying from a large value at the surface to approximately zero in the interior of the fluid layer. This being the case, we would suspect that maintained non-cellular convection is an intrinsically non-linear phenomenon. To show this, we average the steady-state energy equation (6) over a horizontal plane.

$$\iint \underline{u} \cdot \nabla T \, dxdy = \iint \nabla^2 T \, dxdy$$

Here, the integrations are taken over an average horizontal wavelength of the flow pattern. We now express the temperature as the sum of a mean part and a fluctuating part. That is, we write

$$T(x, y, z) = \widetilde{T}(z) + \theta(x, y, z)$$

where

$$\iint \widetilde{T} \, dxdy = \overline{T}$$

and

$$\iint \theta \, dxdy = 0 \ .$$

In view of the conservation of mass, the velocity will have zero horizontal average. The energy balance thus becomes

$$\iint (w \frac{d\widetilde{T}}{dz} + \underline{u} \cdot \nabla\theta) dxdy = \iint \left(\frac{d^2\widetilde{T}}{dz^2} + \nabla^2\theta \right) dxdy \ .$$

Since $\underline{u}$ and θ represent fluctuating quantities in x and y , they may be expanded in Fourier series so that the energy balance may be simplified to give

$$\iint w \frac{d\widetilde{T}}{dz} \, dxdy = \iint \frac{d^2\widetilde{T}}{dz^2} \, dxdy \ ,$$

$$\frac{d}{dz} \iint w \widetilde{T} \, dxdy - \iint \widetilde{T} \frac{\partial w}{\partial z} \, dxdy = \frac{d^2}{dz^2} \iint \widetilde{T} \, dxdy \ .$$

Using again the fact that w is a fluctuating quantity, we have

$$\frac{d}{dz} (\overline{wT}) = \frac{d^2\overline{T}}{dz^2} \ .$$

Integrating once with respect to z , we finally obtain

$$\overline{wT} - \frac{d\overline{T}}{dz} = Q \qquad (73)$$

where Q is the constant heat flux. Equation (73) states that the sum of the averaged convective heat transfer and the averaged conductive heat transfer is a constant for all horizontal planes in the fluid. Now if $d\overline{T}/dz$ varies from a numerically large value at $z = 0$ to zero inside the layer, then $\overline{wT}$ must vary in an equally violent manner to satisfy (73). That is, the non-linear convective terms $\underline{u}\cdot\nabla T$ and $\underline{u}\cdot\nabla\underline{u}$ are of fundamental importance in maintained non-cellular convection.

It is therefore suggested that non-cellular convection is initiated at a Rayleigh number equal to or greater than 1340, depending on the rate of heating, and that the subsequent maintained mode of convection is intrinsically non-linear. Since it appears that a transition from columnar to cellular convection is possible at about $\widetilde{R} = 1708$, at least when the columnar temperature profile is not too far from being linear, then it is likely that columnar convection is initiated at a value of $\widetilde{R}_c$ lying in the range $1340 \leq \widetilde{R}_c \leq 1708$. This means that the heating rate parameter must fall within a certain range. The subsequent steady-state convection may then be achieved at a Rayleigh number which is less than 1708, but which is at a supercritical value for the sustained form of this mode of convection. Thus a reduction in the heating rate is permissible while still maintaining the convective motion. Evaluation of the lower limit of the temperature difference for this steady state mode is outside the scope of the linear stability analysis.

V. SUMMARY AND CONCLUSIONS

The stability of a fluid having a non-uniform and adverse temperature gradient has been analyzed for the response of infinitesimal disturbances.

The following results have been established for the growth of disturbances in a semi-infinite fluid field.

(i) Increasing the Rayleigh number, $R = [\alpha g(T_o^* - T_1^*)d^3]/\kappa\nu$, increases the growth rate and the wave number of the fastest growing disturbance and the spectrum of wave numbers of unstable disturbances.

(ii) Increasing the Prandtl number reduces the absolute growth rate of all disturbances, but does not affect the spectrum of unstable waves.

(iii) Disturbances for which the wave number satisfies the inequality $a \geq R^{1/4}$ will be damped out.

The velocity and temperature perturbations of the associated motion of these disturbances have certain characteristics as follows.

(iv) The velocity and temperature perturbations both penetrate the stable region of fluid more deeply at smaller values of the supercritical Rayleigh number.

(v) The velocity perturbation penetrates more deeply than the temperature perturbation.

(vi) Increasing the Prandtl number increases the velocity penetration and decreases the temperature penetration.

We have established the following results for marginal stability of infinitesimal disturbances.

(vii) For a semi-infinite fluid, the critical Rayleigh number $[\alpha g(T_o^* - T_1^*)d^3]/\kappa\nu$ is 32.

(viii) In a finite fluid layer, the effect of the rate of heating may be to slightly decrease the critical Rayleigh number $\tilde{R}_c = [\alpha g(T_o^* - T_1^*)h^3]/\kappa\nu$, or it may be to increase $\tilde{R}_c$ considerably over the slow heating value of 1707.8.

(ix) The minimum value of $\tilde{R}_c$ was found to be 1340, which is in close agreement with experimental observations.

The stability of an initially isothermal, finite fluid layer under constant flux heating was examined. The results are in agreement with experimentally obtained results. The principal features were found to be as follows.

(x) Instability will set in for heating rates such that $(\alpha g Q h^4)/(\kappa\nu k) \geq 1708$.

(xi) For $1708 < (\alpha g Q h^4)/(\kappa\nu k) < 5500$, the value of the critical Rayleigh number is reduced over that for the slowest possible heating rate which leads to instability.

(xii) For $(\alpha g Q h^4)/(\kappa\nu k) > 500$, the value of the critical Rayleigh number is increased and continues to increase indefinitely as the heating rate increases.

A finite fluid layer whose lower surface temperature is increasing uniformly with time was also studied, and the results agree with experiments. The main features for this type of heating are given below.

(xiii) For heating rates such that $(\alpha g \beta h^5)/(\kappa^2\nu) < 300$, the critical Rayleigh number is independent of the rate of heating.

(xiv) For heating rates in the range $300 < (\alpha g \beta h^5)/(\varkappa^2 \nu) < 16,000$, the critical Rayleigh number is reduced over that for slow heating rates.

(xv) For $(\alpha g \beta h^5)/(\varkappa^2 \nu) > 16,000$, the value of the critical Rayleigh number is increased and continues to increase indefinitely as the rate of heating increases.

The physical phenomenon of columnar instability is regarded as a sustained mode of thermal convection which arises from infinitesimal disturbances becoming unstable during time dependent heating. The steady flow field is intrinsically non-linear.

REFERENCES

BÉNARD, H. (1900). Les tourbillons cellulaires dans une nappe liquide. Revue générale des Sciences pures et appliquées, 11, 1261-71 and 1309-28.

BÉNARD, H. (1901). Les tourbillons cellulaires dans une nappe liquide transportant de la chaleur par convection en régime permanent. Ann. Chim. Phys., 23, 62-144.

BÉNARD, H. and AVSEC, D. (1938). Travaux récents sur les tourbillons cellulaires et les tourbillons en bandes. Applications à l'astrophysique et à la météorologie. J. Phys. Rad., Ser. 7, 9, 486-500.

CHANDRA, K. (1938). Instability of fluids heated from below. Proc. Roy. Soc. A, 164, 231-42.

CHANDRASEKHAR, S. (1961). Hydrodynamic and Hydromagnetic Stability. Oxford University Press.

DASSANAYAKE, D. T. E. See SUTTON, O. G. (1950).

FOSTER, T. D. (1965a). Stability of a homogeneous fluid cooled uniformly from above. Phys. Fluids, 8, 1249-57.

FOSTER, T. D. (1965b). Onset of convection in a layer of fluid cooled from above. Phys. Fluids, 8, 1770-74.

FROMM, J. E. (1965). Numerical solutions of the non-linear equations for a heated fluid layer. Phys. Fluids, 8, 1757-69.

GORKOV, L. P. (1958). Steady convection in a plane liquid layer near the critical heat-transfer point. Sov. Phys. JETP, 6, 311-15.

GRAAF, J. G. A. DE, and HELD, E. F. M. VAN DER (1953). The relation between heat transfer and the convection phenomena in enclosed plane air layers. App. Sci. Res. A, 3, 393-409.

GRAHAM, A. (1933). Shear patterns in an unstable layer of air. Phil. Trans. A, 232, 285-96.

GRIBOV, V. N., and GUREVICH, L. E. (1957). On the theory of the stability of a layer located at a superadiabatic temperature gradient in a gravitational field. Sov. Phys. JETP, 4, 720-29.

HERRING, J. R. (1963). Investigation of problems in thermal convection. J. Atmos. Sci., 20, 325-38.

JEFFREYS, H. (1926). The instability of a layer of fluid heated from below. Phil. Mag., Ser. 7, 2, 833-44.

JEFFREYS, H. (1928). Some cases of instability in fluid motion. Proc. Roy. Soc. A, 118, 195-208.

JEFFREYS, H. (1930). The instability of a compressible fluid heated below. Proc. Camb. Phil. Soc., 26, 170-72.

KUO, H. L. (1961). Solution of the non-linear equations of cellular convection and heat transport. J. Fluid Mech., 10, 611-34.

LICK, W. (1965). The instability of a fluid layer with time-dependent heating. J. Fluid Mech., 21, 565-76.

LOW, A. R. (1929). On the criterion for stability for a layer of fluid heated from below. Proc. Roy. Soc. A, 125, 180-95.

MALKUS, W. V. R. (1954). Discrete transitions in turbulent convection. Proc. Roy. Soc. A, 225, 185-95.

MALKUS, W. V. R. and VERONIS, G. (1958). Finite-amplitude cellular convection. J. Fluid Mech, 4, 225-60.

MINER, R. W. (ed.) (1947). Convection patterns in the atmosphere and ocean. Ann. N. Y. Acad. Sci., 48, 705-844.

MORTON, B. R. (1957). On the equilibrium of a stratified layer of fluid. Quart. J. Mech. App. Math., 10, 433-47.

NAKAGAWA, Y. (1960). Heat transport by convection. Phys. Fluids, 3, 82-86.

PALM, E. (1960). On the tendency towards hexagonal cells in steady convection. J. Fluid Mech., 8, 183-92.

PALM, E. and ØIANN, H. (1964). Contribution to the theory of cellular thermal convection. J. Fluid Mech., 19, 353-65.

PELLEW, A. and SOUTHWELL, R. V. (1940). On maintained convective motion in a fluid heated from below. Proc. Roy. Soc. A, 176, 312-43.

RAYLEIGH, Lord (1916). On convective currents in a horizontal layer of fluid when the higher temperature is on the under side. Phil. Mag., 32, 529-46; also Scientific Papers, 6, 432-46 (1920).

SCHMIDT, R. J. and MILVERTON, S. W. (1935). On the stability of a fluid when heated from below. Proc. Roy. Soc. A, 152, 586-94.

SCHMIDT, R. J. and SAUNDERS, O. A. (1938). On the motion of a fluid heated from below. Proc. Roy. Soc. A, 165, 216-28.

SEGEL, L. A. (1962). The non-linear interaction of two disturbances in the thermal convection problem. J. Fluid Mech., 14, 97-114.

SEGEL, L. A. (1965a). The structure of non-linear cellular solutions to the Boussinesq equations. J. Fluid Mech., 21, 345-58.

SEGEL, L. A. (1965b). The non-linear interaction of a finite number of disturbances to a layer of fluid heated from below. J. Fluid Mech., 21, 359-84.

SEGEL, L. A. and STUART, J. T. (1962). On the question of the preferred mode in cellular thermal convection. J. Fluid Mech., 13, 289-306.

SILVESTON, P. L. (1958). Wärmedurchgang in waagerechten Flüssigkeitsschichten, I and II. Forsch. Arb. Ing. Wes , 24, 29-32 and 59-69.

SOBERMAN, R. K. (1959). Onset of convection in liquids subject to transient heating from below. Phys. Fluids, 2, 131-38.

SPANGENBERG, W. G. and ROWLAND, W. R. (1961). Convective circulation in water induced by evaporative cooling. Phys. Fluids, 4, 743-50.

SPARROW, E. M., GOLDSTEIN, R. J., and JONSSON, V. K. (1964). Thermal instability in a horizontal fluid layer; effect of boundary conditions and non-linear temperature profile. J. Fluid Mech., 18, 513-28.

SUTTON, O. G. (1950). On the stability of a fluid heated from below. Proc. Roy. Soc. A, 204, 297-309.

THOMSON, J. (1882). On a changing tesselated structure in certain liquids. Proc. Phil. Soc. Glasgow, 13, 464-68; also Papers in Physics and Engineering, Cambridge University Press (1912).

TIPPELSKIRCH, H. VON (1956). Über Konvektionspellen, inbesondere im flüssigen Schwefel. Beitr. Phys. Atmos., 29, 27-54.

VERONIS, G. (1963). Penetrative convection. Astrophys. J., 137, 641-63.